International Journal of Pharmaceutics 605 (2021) 120820

Contents lists available at ScienceDirect

International Journal of Pharmaceutics

journal homepage: www.elsevier.com/locate/ijpharm

Fabrication and evaluation of artemether loaded polymeric nanorods obtained by mechanical stretching of nanospheres

Atharva R. Bhide, Anil B. Jindal *

Department of Pharmacy, Birla Institute of Technology and Science Pilani, Pilani Campus, Jhunjhunu, Rajasthan 333031, India

ARTICLE INFO

Keywords:
Nanoprecipitation
Polymeric nanoparticles
Nonspherical nanoparticles
Antimalarial drug
Film stretching method

ABSTRACT

The objective of the present study was to prepare and evaluate artemether-loaded poly (lactic-co-glycolic acid) (PLGA) nanorods by mechanical stretching of nanospheres. Artemether-loaded PLGA nanospheres were prepared by the standard nanoprecipitation method. To prepare the nanorods, nanospheres (129 nm) were embedded in polyvinyl alcohol film. The film was stretched by using an *in-house* fabricated film stretching apparatus in one dimension at the rate of 10 mm/min in acetone or silicon oil. Nanorods were recovered by dissolving the film in Milli-Q-water after stretching. The effect of film thickness (100 μm vs 150 μm), the ratio of lactide to glycolide in PLGA (50:50 vs 75:25), extent of stretching (2x vs 4x), on the aspect ratio of the nanorods was studied. A sustained release of artemether was observed from both nanospheres and nanorods with almost 85% drug release at the end of 72 h. In cytotoxicity study, almost 90% cell viability was found when THP-1 cells were treated with artemether, nanospheres, and nanorods equivalent to 0.001 to 100 μg/mL of artemether. At all the concentrations of artemether, nanorods showed less haemolysis of RBCs than the nanospheres. Artemether-loaded PLGA nanorods could be successfully prepared by the film stretching method for intravenous delivery of antimalarial drugs.

1. Introduction

Recently, particle shape has been recognized as an important parameter to design the nanocarriers for site-specific drug delivery. The *in vivo* journey of nonspherical nanocarriers largely depends upon the shape and the dimensions of the particle (Jindal, 2017). Nanocarriers, based on the particle shape, have shown a significant difference in several biological processes including phagocytosis (Champion and Mitragotri, 2009), cellular uptake mechanism and kinetics (Jurney et al., 2017), particle-cell interaction (Dasgupta et al., 2014), intracellular distribution of the particles (Yoo et al., 2010), margination of the particles in the blood vessels (Jurney et al., 2017) and tissue distribution of particles (Zhu et al., 2019). Moreover, the impact of particle shape on the cytotoxicity and *in vivo* antitumor efficacy of anticancer agents have been extensively investigated (Wang et al., 2019). It has also been reported that the nonspherical nanocarriers (needle-shaped) showed improved cytoplasmic delivery of siRNA as compared to its spherical counterpart (Kolhar et al., 2011).

The significant impact of the nanocarrier geometry on the *in vivo* performance of the nanoparticles directed the researchers towards the exploitation of methods for the fabrication of nonspherical nanoparticles. Several techniques including PRINT® (Rolland et al., 2005), microfluidics (Dendukuri et al., 2005), modified nanoprecipitation (Jindal and Devarajan, 2015), solvent evaporation (Zhang et al., 2021), sol–gel technique (Shukla and Seal, 2004), co-precipitation (Aphesteguy et al., 2015), template assembly (Mathaes et al., 2015), self-assembly (Mhatre and Sodha, 2019) and solvent moulding methods (Caldorera-Moore et al., 2010) have been reported for the design of nonspherical nanoparticles of varied geometries.

Ho et. al. reported the fabrication of ellipsoidal shaped polystyrene-based micro- and nanoparticles of different aspect ratio (AR) using the film stretching method (Ho et al., 1993). Later, Champion et. al. also used the same method to prepare polystyrene-based nonspherical micro- and nanoparticles of more than 20 different shapes and sizes ranging from 60 nm to 30 μm (Champion et al., 2007). In another study, Palazzo et al. reported the fabrication of elongated chitosan coated poly

Abbreviations: % DL, % drug loading; % EE, % entrapment efficiency; AR, aspect ratio; EDTA, ethylenediamine tetraacetic acid; FBS, foetal bovine serum; HPLC, high performance liquid chromatography; MTT, 3-(4,5-dimethylthiazol-2-yl)-2,5-diphenyl tetrazolium bromide; MW, molecular weight; PLGA, poly (lactic-co-glycolic acid); PMA, phorbol 12-myristate 13-acetate; PVA, polyvinyl alcohol; SLS, sodium lauryl sulphate.

* Corresponding author at: Department of Pharmacy, Birla Institute of Technology and Science (BITS), Pilani Campus, Pilani 333031, Rajasthan, India.
E-mail addresses: anil.jindal@pilani.bits-pilani.ac.in, anil_jndl@yahoo.co.in (A.B. Jindal).

https://doi.org/10.1016/j.ijpharm.2021.120820
Received 9 April 2021; Received in revised form 4 June 2021; Accepted 7 June 2021
Available online 22 June 2021

(alkylcyanoacrylate) nanoparticles by mechanical stretching of water-soluble film (Palazzo et al., 2017). Although, the film stretching method has been investigated for the fabrication of polystyrene-based nonspherical nanoparticles, yet there are very few reports present on the fabrication of biodegradable polymer-based nonspherical nanoparticles. Cao et. al. reported fabrication of functionalized biodegradable poly(lactic-co-glycolic acid) (PLGA) nanorods of the dimensions 380 × 100 (nm) with AR of 4 using the film stretching method (Cao et al., 2019). In another study, Castoldi et al. prepared drug-loaded functionalized PLGA nanorods with an AR of 2.6. They observed significantly enhanced intracellular inhibition of bacteria by nanorods as compared to nanospheres (Castoldi et al., 2019). To enable successful translation of the nanocarriers from lab to clinic, fabrication of nonspherical nanoparticles using biodegradable polymers is extremely important. To the best of our knowledge, biodegradable polymer based nonspherical nanoparticles encapsulating antimalarial drugs have not been attempted yet.

Therefore, the objective of the present study was the preparation and evaluation of artemether-loaded PLGA based nanorods by mechanical stretching of nanospheres. In the present study, artemether-loaded PLGA nanospheres were prepared by the standard nanoprecipitation method and loaded into the polyvinyl alcohol (PVA) film. The nanosphere loaded film was then stretched using an *in-house* fabricated film stretching apparatus to form nanorods by mechanical stretching of nanospheres. The influence of process parameters and material related properties on the AR of nanorods was investigated. The nanorods were further evaluated for *in vitro* release, cytotoxicity, and haemolysis.

2. Materials and methods

2.1. Materials

Artemether (>98.0%) was purchased from Tokyo Chemical Industry Co. Ltd. (Tokyo, Japan). Poly(lactic-co-glycolic) acid (PLGA) (50:50, MW 30,000–60,000) and (75:25, MW 4000–15,000), polyvinyl alcohol (PVA, MW 9000–10,000) were purchased from Sigma-Aldrich Chemicals Company (Missouri, United States). Glycerol was purchased from S D Fine-Chem Ltd (Mumbai, India). Silicon oil was purchased from Rankem™ (Bangalore, India). Trehalose was purchased from Spectrochem (Mumbai, India). Emplura® grade acetone was procured from Merck Life Science Pvt. Ltd. (Mumbai, India). Water was obtained from Milli-Q system (Millipore GmbH, Germany). All other chemicals, solvents, and reagents utilized were either HPLC or analytical grade.

2.2. Methods

2.2.1. Preparation of artemether loaded PLGA nanospheres

Artemether loaded PLGA nanospheres were prepared by the standard nanoprecipitation method. Briefly, PLGA (75 mg) and artemether (5 mg or 10 mg) were dissolved in acetone (5–15 ml) to prepare the organic phase. The aqueous phase was prepared by dissolving the PVA (molecular weight 9000–10,000) (0.25–1% w/v) in Milli-Q water at 65 C. The organic phase was added drop-wise to the aqueous phase under constant stirring (400 rpm). Thereafter, the organic phase was evaporated using a rotary vacuum evaporator (Buchi Rotavapor, Switzerland) at 40 C under reduced pressure. After the evaporation of the organic phase, the aqueous dispersion was centrifuged at 20,000 rpm for 40 min to separate the artemether loaded PLGA nanospheres. The obtained pellet was redispersed in 1 ml of Milli-Q water by sonication. Nanospheres were characterized for particle size, polydispersity index (PDI), % entrapment efficiency, particle shape and % drug loading. The artemether loaded PLGA nanospheres were freeze-dried using trehalose (10% w/v) as a cryoprotectant and stored at 4 C until further use.

2.2.2. Preparation of artemether loaded PLGA nanorods

Artemether loaded PLGA nanorods were prepared as reported previously by Champion et. al. with modification (Champion et al., 2007). Briefly, a film-forming solution was prepared by dissolving PVA (5% w/v) and glycerol (2.5% w/v) in Milli-Q water. Thereafter, 1 ml of aqueous dispersion of artemether loaded PLGA nanospheres (equivalent to 10 mg of artemether) was added to the above film-forming solution (10 ml) under stirring which was then added to a 6 × 6 (cm) glass mould and dried at room temperature for 24 h to form the artemether loaded PLGA nanospheres embedded polymeric film. The film was stretched by using an *in-house* fabricated film stretching apparatus (Fig. 1) in one dimension at the rate of 10 mm/min in acetone or silicon oil (65°C). In the case of acetone, the film was immersed in acetone for 15 min, removed, and stretched in the air. While in case of heat stretching, the film was immersed in hot silicon oil, for 15 min and stretched while still in the oil. The extent of stretching was varied from 2- to 4-fold of the initial length of the film. After stretching, the film was removed from the apparatus and dissolved in Mill-Q-water. The particles were washed with water to remove the PVA absorbed onto the particle surface and separated by centrifugation. The particles were freeze-dried and stored at 4°C until further use.

2.3. Characterization of nanospheres and nanorods

2.3.1. Particle size and PDI

The aqueous nanodispersion of artemether loaded nanospheres was centrifuged at 20,000 rpm for 40 min (Sorvall 150 + Micro Ultracentrifuge, United States). The supernatant was removed, and the pellet was re-dispersed in Milli-Q water to get a dispersion of 83.7 mg/ml concentration. The particle size and PDI were determined using Malvern Nano ZS (Malvern Instruments Ltd. UK) after appropriate dilution of the re-dispersed sample.

2.3.2. % Entrapment efficiency (EE)

The supernatant obtained after centrifugation of the nanoformulation was analysed by the RP-HPLC method reported previously by our group (Bhide et al., 2020). %EE was calculated using Eq. (1)

$$\%EE = \frac{Totalquantityofdrugused - Drugcontentinthesupernatant}{Totalquantityofdrugused} x100 \quad (1)$$

2.3.3. % Drug loading

The drug loading is calculated by determining the entrapped drug in the formulation. It can be expressed as the mass ratio of artemether to the artemether loaded nanospheres (Liu et al., 2020). The % drug loading can be calculated using Eq. (2)

$$\%DL = \frac{Totalquantityofdrugentrapped}{(Totalquantityofdrugused + Totalquantityofpolymerused)} x100 \quad (2)$$

2.3.4. Drug content

The accurately weighed (10 mg) of the lyophilized nanorods was dispersed in 1 ml of methanol and vortexed and sonicated for 5 min. The dispersion was centrifuged and supernatant was then acid treated and analysed using the RP-HPLC method previously reported by our group (Bhide et al., 2020).

2.3.5. Field emission scanning electron microscopy

Aliquot of aqueous dispersion of nanospheres or nanorods was placed onto the coverslip and dried at room temperature. The coverslip was then placed on the metal stub and gold coated for 45 sec by sputter coater (Quorum Technologies Q150TES, East Sussex, England). The coated nanoparticles were then analysed by FEI scanning electron microscope (Hillsboro, Washington) at 20 kV high vacuum, with 9.0 as the spot size and the scale set to 300 to 1000 nm.

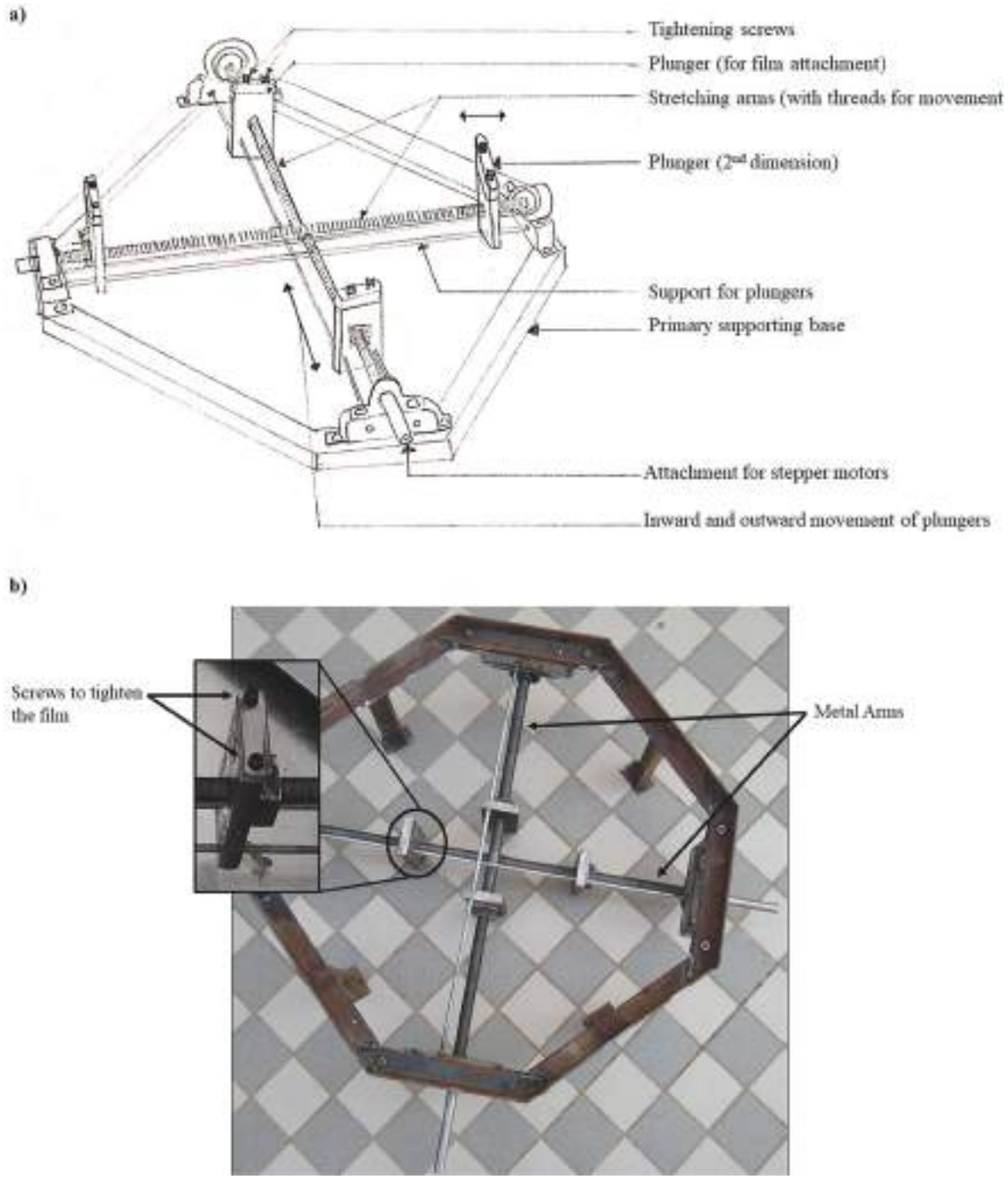

Fig. 1. *In house* fabricated film stretching apparatus a) Schematic representation of the apparatus b) Image acquired by digital camera.

2.4. Calculation of shape descriptors of nanorods

Feret diameter, minor Feret diameter, AR, major axis, and minor axis were used as shape descriptors to characterize the nanorods. The shape descriptors were determined from the SEM images of the nanorods using Fiji ImageJ software (Version 1.52p).

2.4.1. Feret diameter and minor Feret diameter

Feret diameter is the distance between two parallel tangents drawn perpendicular to two ends of the particle having maximal distance from each other. While, in case of minor Feret diameter, the distance calculated is between two endpoints having minimal distance from each other (Baybay et al., 2020; Yu and Hancock, 2008). It is primarily calculated for asymmetrical particles. Feret diameter and minor Feret diameter of a nanorod are depicted schematically in Fig. 2.

2.4.2. Major axis, minor axis and aspect ratio

Major axis is the distance of the segment connecting the farthest points of the particle comprising its maximum length. While minor axis is the distance of the segment connecting the closest points of the particle. Aspect ratio is the ratio of the major axis to the minor axis of the particle. Major axis and minor axis of a nanorod are depicted schematically in Fig. 2.

2.4.3. Size distribution of nanorods

The percentage frequency of distribution of major and minor axis of

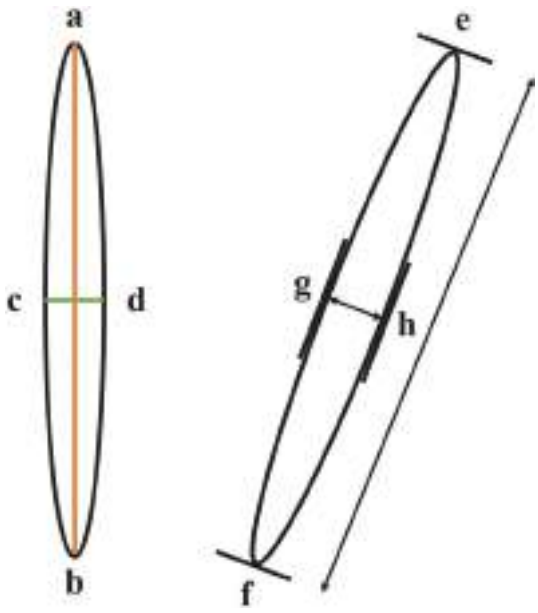

Fig. 2. Schematic representation of the shape descriptors used for the characterisation of a rod-shaped particle. Segment a-b and c-d represent the major axis and minor axis of the nanorod, respectively. Distance between point e to f and point g to h represent the Feret diameter and minor Feret diameter.

nanorods was determined and data was represented in the form of size-frequency distribution curve by plotting percentage frequencies of various particles against particle size. The D_{10}, D_{50} and D_{90} values were calculated from size-frequency distribution curve.

2.5. Evaluation of nanospheres and nanorods

2.5.1. In vitro release study

In vitro release of artemether from nanospheres and nanorods was determined using the dialysis bag method as described previously with modifications (Raina et al., 2017). Nanospheres or nanorods (equivalent to 5 mg of artemether) were dispersed in 2 ml of Milli-Q water and was filled in a dialysis bag (SnakeSkin^{TM}, 3.5 K MWCO, Thermo Scientific, USA). The dialysis bag was immersed in 50 ml of 10 mM phosphate buffer pH 7.4 with sodium lauryl sulphate (SLS) (1% w/v) for 72 h under stirring (100 rpm) at 37 C. SLS was used to maintain the sink conditions during the release studies as reported previously by the researchers. (Belew et al., 2020; Pawar et al., 2016; Shende et al., 2017). 2 ml of sample was withdrawn at predetermined time points (0.25, 0.5, 1, 2, 4, 6, 12, 24, 48, and 72 h) and was replaced with an equal amount of fresh media. The samples were analysed by HPLC after pre-column acid treatment as reported previously by our group (Bhide et al., 2020). The study was carried out in triplicate.

2.5.2. Cytotoxicity

THP-1 suspension cell line was cultured in RPMI 1640 media with 10% (foetal bovine serum) FBS and gentamycin (0.005%) in a T-75 culture flask till an optimal cell count was obtained. THP-1 cells were seeded in a 96-well plate with phorbol 12-myristate 13-acetate (PMA) to differentiate it at a count of 10,000 cells per well. The cells were incubated with artemether, nanospheres (artemether equivalent to 0.001, 0.01, 0.1, 1, 10, 100, and 200 μg/mL), nanorods (artemether equivalent to 0.001, 0.01, 0.1, 1, 10, 100, and 200 μg/mL), blank nanospheres and blank nanorods for 24 h. Then, 100 μL of 3-(4,5-dimethylthiazol-2-yl)-2,5-diphenyl tetrazolium bromide (MTT) solution (0.5 μg/mL) was added to each well and incubated for 4 h. After 4 h, the MTT solution was replaced by DMSO and the absorbance was recorded at 540 nm using an Epoch ELISA plate reader (BioTek, Winooski, United States). % cell viability was calculated by using the Eq. (3)

$$\%cell\ viability = \frac{(absorbanceofsample - absorbanceofblank)}{(absorbanceofcontrol - absorbanceofblank)} x100 \quad (3)$$

2.5.3. Haemolysis study

In vitro haemolysis study was carried out as reported previously by our group (Jindal et al., 2020). Blood was collected from Wistar rats in microcentrifuge tubes containing Ethylenediamine tetraacetic acid (EDTA) (10% w/v). Red blood cells (RBCs) were collected after centrifugation of blood at 1000 rpm for 5 min and washed thrice with normal saline. 5 μL of the packed erythrocytes were treated with 95 μL of the nanospheres (artemether equivalent to 0.001, 0.01, 0.1, 1, 10, 100, and 200 μg/mL) or nanorods (artemether equivalent to 0.001, 0.01, 0.1, 1, 10, 100, and 200 μg/mL). Thereafter, the samples were centrifuged at 1000 rpm for 5 min and the supernatant was analysed at 540 nm using an Epoch ELISA plate reader (BioTek, Winooski, United States). Normal saline and Milli-Q water were used as a negative control and positive control, respectively, during the study. % haemolysis was calculated using the Eq. (4)

$$\%hemolysis = \frac{absorbanceofthesample}{absorbanceofthepositivecontrol} x100 \quad (4)$$

2.6. Statistical analysis

The data was analysed using a student *t*-test or ANOVA with $p < 0.05$ as a minimal level of significance. All the results expressed in mean ± standard deviation.

3. Results

3.1. Preparation of nanospheres

Artemether loaded PLGA nanospheres were prepared by the nanoprecipitation method. Particle size, PDI, zeta potential, and % EE of nanospheres obtained after varying different parameters are presented in table 1. Particle size, PDI, zeta potential, and % EE were found to be affected by the ratio of organic to aqueous phase, surfactant concentration, and amount of drug used during the preparation of nanospheres. There was an increase in particle size observed when the ratio of aqueous to organic phase was increased from 1:2 to 1:3. Similarly, when the drug amount was increased from 5 mg to 10 mg, particle size was increased from 196 nm to 214 nm. Furthermore, the effect of surfactant concentration on particle size was found to be dependent upon the amount of drug used in the study. Surprisingly, at lower drug concentration (5 mg), an increase in particle size was observed with an increase in surfactant concentration, while, in the case of 10 mg drug, particle size was decreased from 245 nm to 196 nm when surfactant concentration was increased. Moreover, an increase in organic phase to aqueous phase ratio resulted in narrow particle size distribution with a PDI of 0.06 ± 0.01. In all the cases, the zeta potential was found to be less than −15 mV and % EE was found to be more than 70%.

3.2. Preparation of nanorods

PLGA nanospheres of diameter 129.33 ± 3.64 nm were used to obtain nanorods by mechanical stretching after embedded into the PVA film. The film was kept in acetone for 15 min, removed, and stretched in air to obtain nanorods. The effect of various parameters including film thickness (100 μm vs 150 μm), the ratio of lactide to glycolide (50:50 vs 75:25), extent of stretching (2x vs 4x), and liquefaction method (acetone vs heat) on the dimensions of the nanorods including major axis, minor axis, AR, Feret diameter and minor Feret diameter are presented in table 2.

Size-frequency distribution curve of major and minor axis of

Table 1
Particle size, PDI, %EE, %DL and zeta potential of the artemether loaded nanospheres.

Composition Artemether (mg)	PLGA (mg)	PVA (mg)	Acetone (mL)	Aqueous phase (mL)	Particle size (nm)	PDI	Zeta potential (mV)	%EE	% DL
5	75	75	5	15	190.2 ± 18.0	0.06 ± 0.01	−8.0 ± 0.58	78.5 ± 1.8	4.9 ± 0.1
5	75	150	5	15	214.3 ± 6.2	0.238	−1.8 ± 0.22	80.0 ± 0.1	5.0 ± 0.0
10	75	300	10	30	196.8 ± 1.1	0.214	−2.2 ± 0.16	78.3 ± 0.0	9.2 ± 0.0
10	75	150	10	30	245.5 ± 44.5	0.183	−3.2 ± 0.24	80.6 ± 0.4	9.5 ± 0.0
10	75	150	15	30	129.3 ± 3.6	0.06 ± 0.01	−7.4 ± 0.69	86.9 ± 0.2	10.2 ± 0.0

Each value presented as mean ± SD, n = 3.

Table 2
Physicochemical parameters of nanorods obtained by varying the process conditions.

Process conditions					Major axis (nm)	Minor axis (nm)	AR	Feret's diameter (nm)	Minor Feret's diameter (nm)	Drug content (μg/mg)
Film thickness (μm)	PLGA type (lactide: glycolide)	Extent of stretching	Liquefaction method	Incubation period (min)						
100	75:25	4x	Acetone	15	234.1 ± 61.7	61.3 ± 8.7	3.8 ± 0.8	237.2 ± 61.9	77.8 ± 13.3	1.8
150	75:25	4x	Acetone	15	295.1 ± 64.9	58.1 ± 12.0	5.1 ± 0.8	265.4 ± 66.3	59.6 ± 15.2	1.4
100	50:50	4x	Acetone	15	211.3 ± 44.1	61.1 ± 11.6	3.5 ± 0.7	198.1 ± 37.5	67.7 ± 10.4	2.6
100	75:25	2x	Acetone	15	128.1 ± 23.1	61.5 ± 10.3	2.1 ± 0.3	127.5 ± 22.9	61.3 ± 10.4	1.6
100	75:25	4x	Heat*	5	241.7 ± 76.3	140.1 ± 31.3	1.7 ± 0.3	294.0 ± 85.8	157.6 ± 32.8	0.9
100	75:25	2x	Heat*	15	329.6 ± 79.3	92.2 ± 14.9	3.6 ± 0.7	343.0 ± 79.7	98.9 ± 17.8	0.8
100	75:25	4x	Heat*	15	510.7 ± 114.6	102.0 ± 23.7	5.1 ± 0.9	559.5 ± 102.8	119.3 ± 28.8	3.2

*In case of heat treatment, 65 °C temperature was used.

nanorods obtained from stretching of nanospheres after solvent treatment are presented in Fig. 3 (a-d) and Fig. 3 (e-h) respectively. SEM images of nanospheres and nanorods obtained from mechanical stretching of nanospheres after solvent treatment are presented in Fig. 3 (i-m). AR of nanorods was found to be 3.82 ± 0.82 when nanospheres were stretched to 4x of its initial length in a thin film (100 μm) . While in the case of thick film (150 μm), nanorods with AR 5.13 ± 0.85 were produced. The particles were observed to be uniformly elongated in both the cases ($D_{90\ major}$ = 340 nm and $D_{90\ minor}$ = 75 nm for 100 μm film and $D_{90\ major}$ = 395 nm and $D_{90\ minor}$ = 80 nm for 150 μm film). Moreover, it has been observed that as the film thickness was increased, the major axis was found to be increased (1.26-fold) while the minor axis was decreased (1.05-fold). To study the impact of the extent of stretching on the nanorods, the film (100 μm) was stretched to 2x and 4x to its initial length. It was observed that the film which was stretched to 2x produced nanorods with an AR = 2.11 ± 0.35, while nanorods with AR = 3.82 ± 0.82 were obtained from the film which was stretched 4x of its initial length ($D_{90\ major}$ = 170 nm and $D_{90\ minor}$ = 75 nm for 2x stretched film). Moreover, an almost 1.82-fold increase in the major axis of nanorods was obtained when film was stretched 4x as compared to the stretching extent of 2x. However, there was no effect of stretching extent on the minor axis of nanorods observed. Impact of lactide: glycolide ratio in the PLGA on the dimension of nanorods was also studied. Nanospheres prepared using PLGA (lactide: glycolide 50:50 or lactide: glycolide 75:25) were embedded in the film and stretched 4x to the initial length of the film. In both the cases, the AR of nanoparticles was found to be 3.52 ± 0.71 and 3.82 ± 0.82 respectively. ($D_{90\ major}$ = 300 nm and $D_{90\ minor}$ = 80 nm for PLGA 50:50).

Size-frequency distribution curve of major and minor axis of nanorods obtained from stretching of nanospheres after heat treatment are presented in Fig. 4 (a-c) and Fig. 4 (d-f) respectively SEM images of nanospheres and nanorods obtained from mechanical stretching of nanospheres after heat treatment are presented in Fig. 4 (g-j). Replacing acetone with heat to liquefy the particles also resulted in the formation of nanorods. However, the incubation time of the film in the oil exerted a significant impact on the shape and dimensions of the particles. Oval-shaped particles with AR = 1.72 ± 0.33 were obtained when the film was incubated for 5 min and stretched 4x of its initial length in the oil. While in the case of incubation time of 15 min, nanorods of AR = 5.07 ± 0.92 were produced ($D_{90\ major}$ = 355 nm and $D_{90\ minor}$ = 195 nm for film incubated for 5 min and $D_{90\ major}$ = 700 nm and $D_{90\ minor}$ = 130 nm for film incubated for 15 min). Furthermore, AR of nanorods was found to be 3.60 ± 0.75 and 5.07 ± 0.92 when the film was stretched 2x and 4x of its initial length, respectively ($D_{90\ major}$ = 430 nm and $D_{90\ minor}$ = 116 nm for 2x stretched film). The method of liquefaction of the nanosphere during stretching exerted a significant impact on the AR of nanorods.

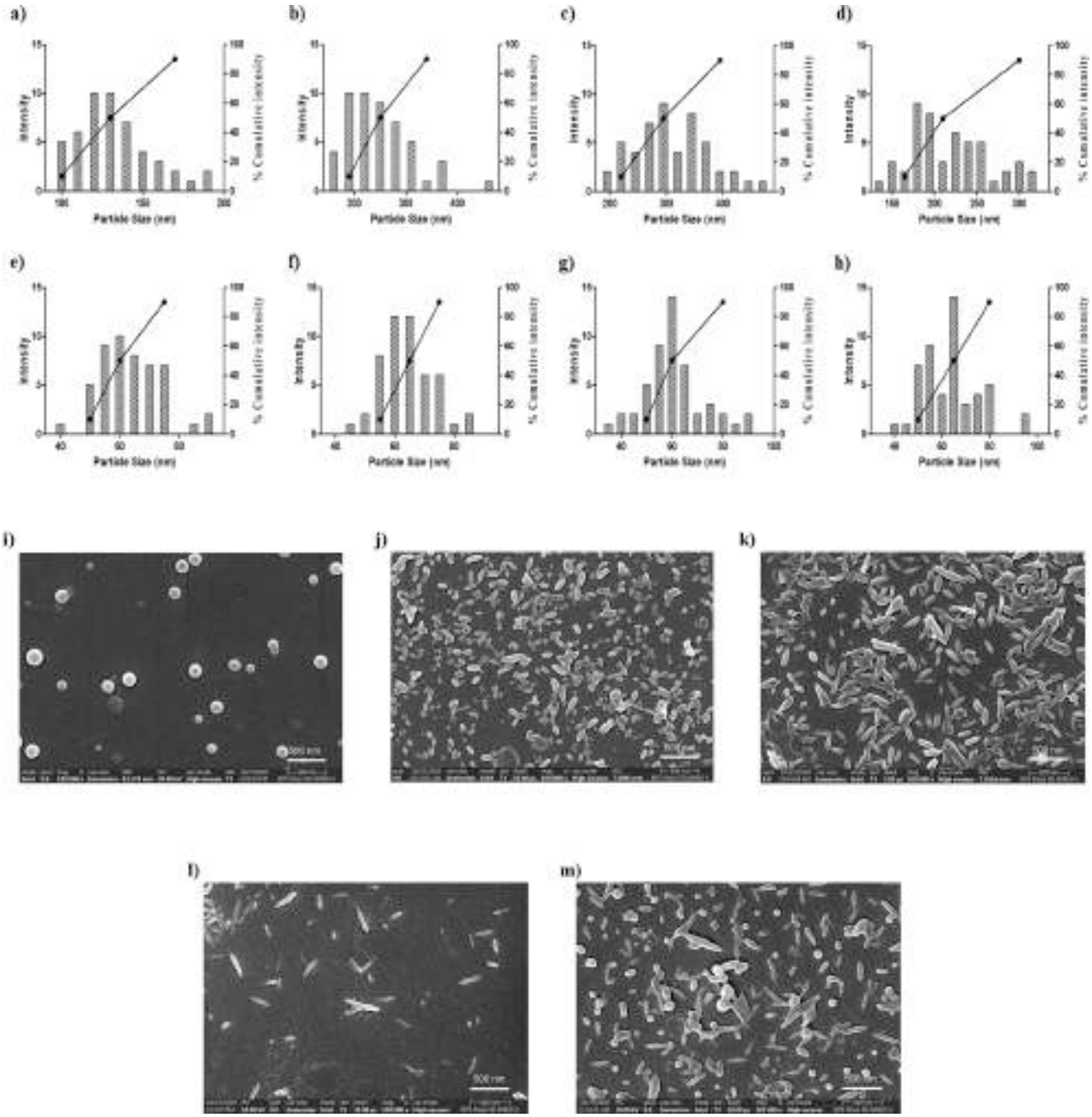

Fig. 3. Characterisation of size and shape of the nanorods obtained from mechanical stretching of nanospheres after solvent treatment. Size-frequency distribution curves of major axis (a-d), minor axis (e-h) and SEM images (j-m) of nanorods, (i) of nanospheres; a) major axis, e) minor axis and j) SEM image of nanorods (film thickness = 100 μm, L/G ratio = 75: 25, stretching extent = 2x), b) major axis, f) minor axis and k) SEM image of nanorods (film thickness = 100 μm, L/G ratio = 75: 25, stretching extent = 4x), c) major axis, g) minor axis and l) SEM image of nanorods (film thickness = 150 μm, L/G ratio = 75: 25, stretching extent = 4x), d) major axis, h) minor axis and m) SEM image of nanorods (film thickness = 100 μm, L/G ratio = 50: 50, stretching extent = 4x).

When acetone is replaced by heat as a method of liquefaction, an almost 1.44-fold increase in the AR of nanorods was observed. In all the cases, the Feret diameter and minor Feret diameter of nanorods were found to be similar to the major axis and minor axis respectively, indicating that the particles obtained from the film stretching method were symmetric in shape.

% drug loading of the nanospheres and drug content of the nanorods are presented in table 1 and table 2 respectively. The drug content of the nanorods was found to be less as compared to the nanospheres due to the loss of drug during stretching and recovery of the nanorods. The loss of the drug could be avoided by utilizing a solvent which exhibits high affinity for the polymer instead of the drug.

3.3. *In vitro drug release*

Fig. 5a represents the *in vitro* release profile of artemether loaded nanospheres and nanorods. A sustained release of artemether was observed from both nanospheres and nanorods. Till 24 h, the release of artemether from nanorods was found to be significantly slow ($p < 0.05$) as compared to nanospheres. However, almost 85% drug was found to

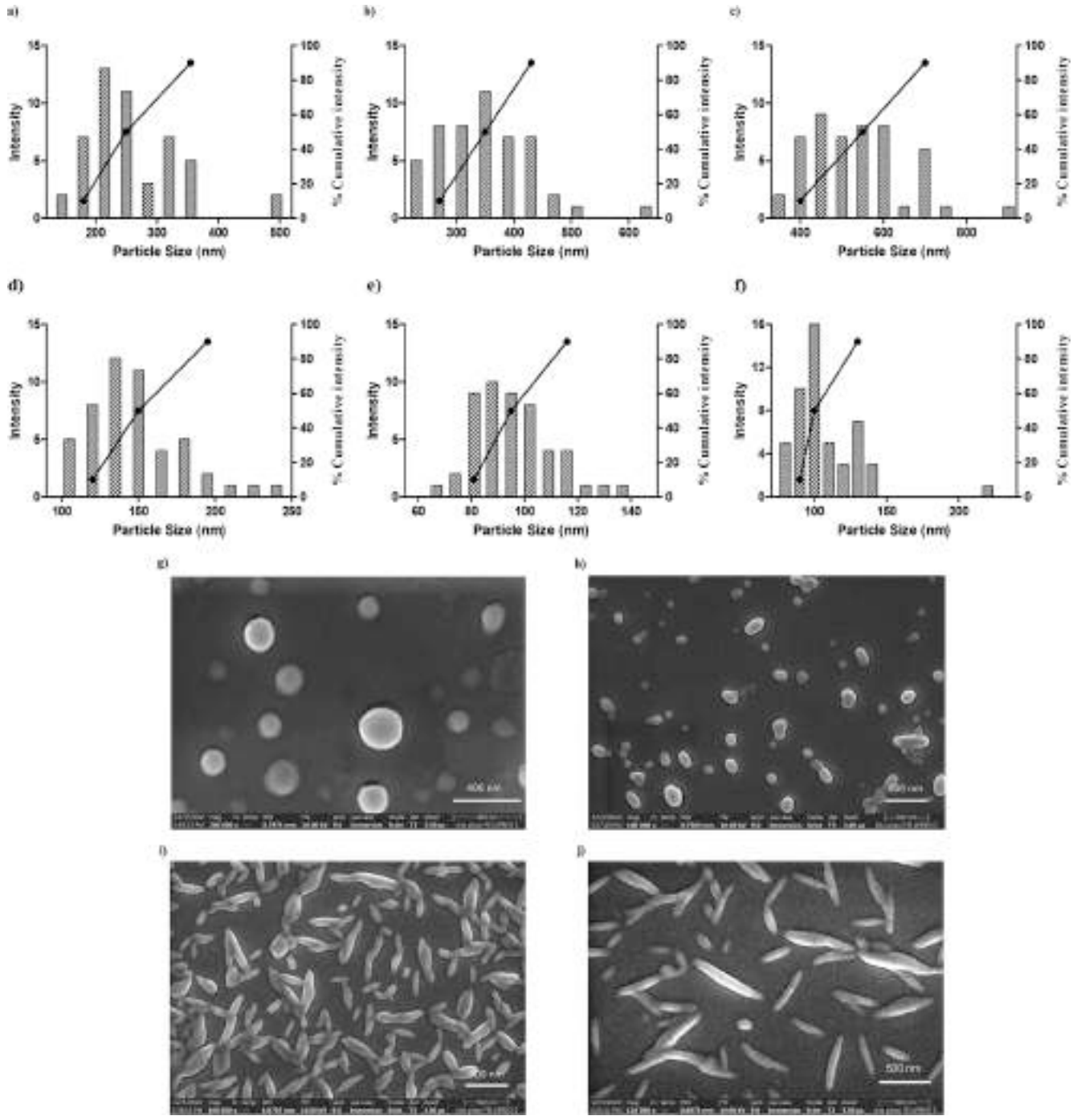

Fig. 4. Characterisation of size and shape of the nanorods obtained from mechanical stretching of nanospheres after heat treatment. Size-frequency distribution curves of major axis (a-c), minor axis (d-f) and SEM images (h-j) of nanorods, (g) of nanospheres; a) major axis, d) minor axis and h) SEM image of nanorods (film thickness = 100 μm, L/G ratio = 75: 25, stretching extent = 4x, incubation time = 5 min), b) major axis, e) minor axis and i) SEM image of nanorods (film thickness = 100 μm, L/G ratio = 75: 25, stretching extent = 2x, incubation time = 15 min), c) major axis, f) minor axis and j) SEM image of nanorods (film thickness = 100 μm, L/G ratio = 75: 25, stretching extent = 4x, incubation time = 15 min).

be released from both nanosphere and nanorods at the end of 72 h.

3.4. Cytotoxicity

In vitro cytotoxicity of both artemether loaded nanosphere and nanorods were studied at different concentrations of artemether using THP-1 monocyte cell line. There was no difference observed in % cell viability of THP-1 cell lines treated with artemether, nanospheres, and nanorods at all the concentrations of the drug (Fig. 5b). Furthermore, almost 90% cell viability was found when THP-1 cells were treated with artemether, nanospheres, and nanorods equivalent to 0.001 to 100 μg/mL of artemether. However, at higher artemether concentration (200 μg/mL), a significant decrease in % cell viability was observed when cells were treated with artemether, nanospheres, and nanorods. Furthermore, at a concentration equivalent to 200 μg/mL of artemether, nanorods showed significantly less % cell viability as compared to nanospheres and free drug.

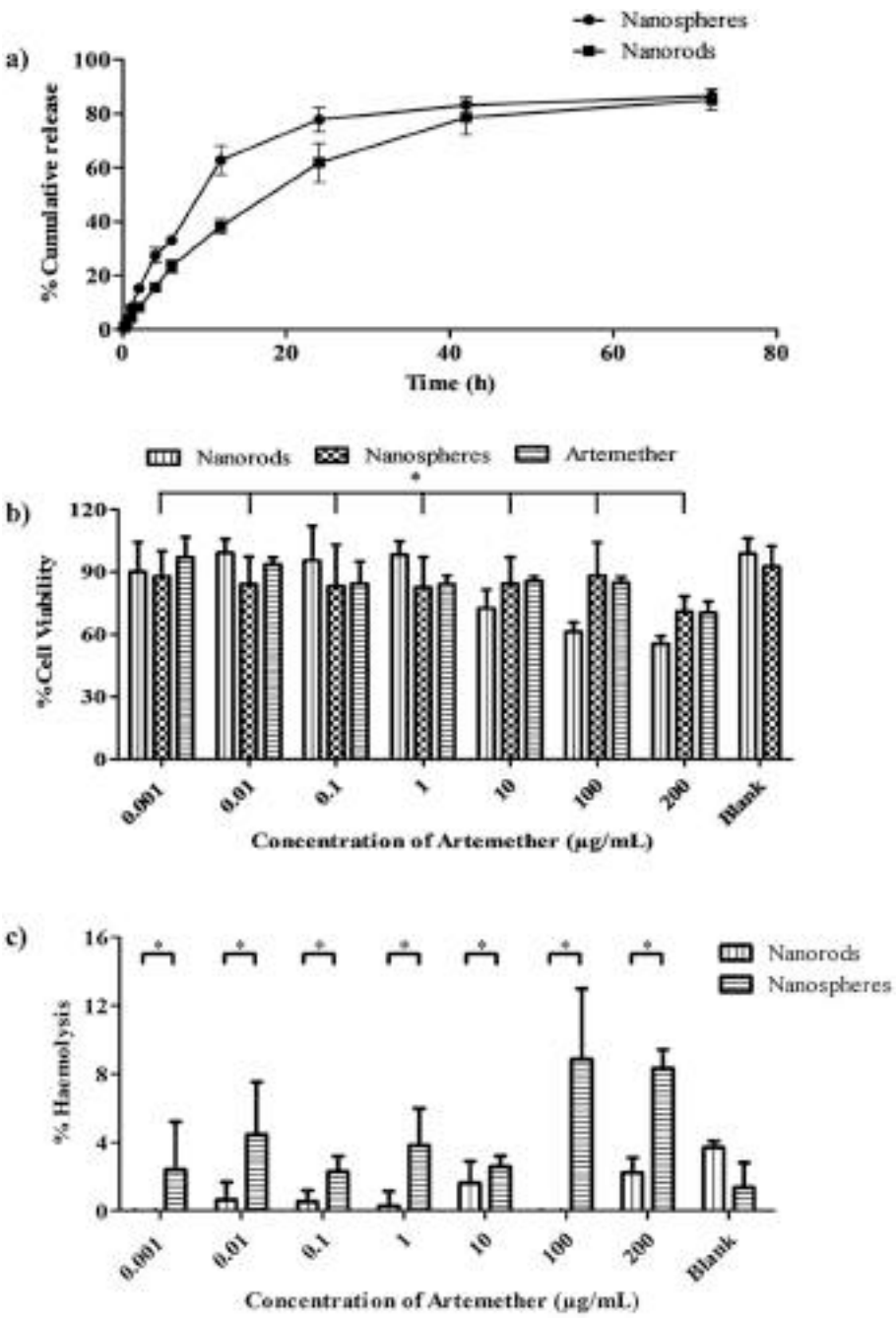

Fig. 5. *In vitro* evaluation of nanospheres and nanorods a) *In vitro* release profile of nanosphere and nanorods in 50 ml of 10 mM phosphate buffer pH 7.4 with sodium lauryl sulphate (SLS) (1% w/v) for 72 h under stirring (100 rpm) at 37 C b) % cell viability of artemether loaded nanospheres, artemether loaded nanorods and artemether free drug at different artemether concentrations in THP-1 monocyte cell lines, c) % haemolysis of RBCs obtained from rat blood after treatment with artemether loaded nanospheres, artemether loaded nanorods at different artemether concentrations, Each data represents the mean ± SD; n = 3; * represents $p < 0.05$.

3.5. *In vitro haemolysis*

In vitro haemolytic potential of nanospheres and nanorods were studied using erythrocytes obtained from rat blood. At all the concentrations of artemether, nanorods showed less haemolysis of red blood cells (RBCs) than the nanospheres (Fig. 5c). However, both nanospheres and nanorods showed<10% haemolysis at all concentrations.

4. Discussion

In case of malaria infection, the plasmodium parasite resides within the RBCs during the erythrocytic phase (Tuteja, 2007). Nanotechnology based delivery systems have been widely investigated for the targeted delivery of antimalarial drugs (Gérard Yaméogo et al., 2020; Sidhaye et al., 2016; Vanka et al., 2018). However, in case of spherical nanoparticles, phagocytosis is a major biological barrier in the targeting delivery of nanoparticles to the *Plasmodium*-infected RBCs. Nonspherical nanoparticles have shown long circulation half-life by evading the macrophage uptake (Arnida et al., 2011; Truong et al., 2015). Moreover, nonspherical nanoparticles also exhibit asymmetric tumbling motion under blood flow causing them to move towards the sides of the vessels, a phenomenon often known as 'margination' (Zhu et al., 2019). Margination of nanoparticles can lead to longer circulation period and interaction with the endothelial cells which could result in longer adhesion duration and generation of drug deport to release the drug for an extended period (Fish et al., 2015). Intravenous administration of nonspherical nanoparticles could provide benefit in malaria therapy either by interacting with the RBCs or contributing to drug release in the bloodstream for a longer duration.

In the present study, we fabricated artemether loaded PLGA

nanorods by mechanical stretching of nanospheres using the film stretching method. A detailed study on the impact of formulation and process-related parameters on the shape and dimensions of biodegradable polymer based nonspherical nanoparticles has not been attempted yet. The film stretching method reported here could generate nanorods of varied aspect ratio depending upon the process conditions. The dimensions of the nanorods (major axis, minor axis, and AR) were dictated by various parameters namely extent of stretching, film thickness, polymer type, and method of liquefaction. We found that thick film produced nanorods with an aspect ratio higher than the nanorods obtained from the thin film. In general, a solid body deforms when it is subjected to opposing forces (Terzopoulos and Fleischer, 1988). In this method, it was expected that deformation of the particles could be the function of stress experienced by the nanospheres during stretching of the polymeric film. Under stress conditions, the change in geometry of the particles was opposed by the cohesive forces present in the PLGA. When the stress on the particles overcome the cohesive forces, nanospheres transform into nanorods. Treatment of PLGA nanospheres embedded PVA film with solvent or heat could have resulted in a decrease in the cohesive forces of the PLGA, which could have ultimately resulted in the elongation of nanospheres. To produce the same amount of strain, thick film required higher stress than the thin film which could have led to the generation of nanorods with high AR from the thick film. However, Champion et. al. reported that AR of the rod-shaped polystyrene particles was decreased with an increase in the film thickness (Champion et al., 2007). The difference in the findings could be due to the difference in the cohesive forces and applied stress during stretching. There was an almost 2-fold increase in the AR and major axis observed with a 2-fold increase in extent of stretching. However, the minor axis of nanorods was not changed with an increase in stretching extent. During the deformation, the stress experienced by the nanospheres was directly proportional to the strain produced in the PVA film by stretching. The increase in the major axis with the preserving dimenssion of the minor axis could be due to the higher stress on the nanospheres in one direction during 4x stretching. AR of nanorods was not affected by an increase in the hydrophobicity of the polymer. However, there was an increase in the major and minor axis of the nanorods observed. It was reported that PVA formed an interconnected network with the PLGA polymer and hence adhered onto the surface of the nanoparticles (Sahoo et al., 2002). Therefore, it was expected that the PVA interacted with the polymer and led to the formation of nanorods. The viscosity of PLGA 50:50 was reported as 0.55 to 0.75 dL/g while that of PLGA 75:25 was 0.14 to 0.22 dL/g. Since viscosity is considered as the resistance in the deformation of the particles, the higher the viscosity, the lower the deformation, and hence the lower the AR of the nanorods. The lower viscosity of the polymer could have contributed to the higher elongation of the nanorods during stretching (Makadia and Siegel, 2011).

The method of liquefaction during stretching produced a significant impact on the dimension of nanorods while the shape of the nanoparticle was not affected. In case of heat treatment, a significant increase in the major axis, minor axis, and AR of nanorods were observed. This could be due to the difference in the extent of reduction in cohesive forces of nanospheres by solvent and heat during stretching. Heating the film at 65 C (higher than the Tg of PLGA) resulted in the conversion of the glassy state to the rubbery state of the polymer. The presence of polymer in the rubbery state at 65 C could have contributed significantly to the elongation of particles. Moreover, the incubation time of the film in the oil also produced a significant impact on the shape and dimension of the particle. As the incubation time was increased from 5 min to 15 min, particle shape was converted from oval to rods which could be due to the decrease in viscosity of the polymer at a longer incubation time. Also, after 5 min of incubation period, the viscosity of the nanoparticles might not be uniform thus leading to an oval shape. Similar observations were reported by the other researchers (Champion et al., 2007; Yoo and Mitragotri, 2010).

The prolonged therapeutic effect of the drug can be obtained by maintaining the plasma concentration of the drug in a therapeutic range for an extended period. Plasma concentration of the drug largely depends upon the release of the drug from the delivery system. Artemether has a half-life of 2 to 3 h (Makanga and Krudsood, 2009) and hence a delivery system capable of releasing the drug for a longer duration is highly desirable to reduce the dosing frequency. In the case of nanocarriers, drug release is dictated by the size, shape, and surface area of the nanoparticles. In general, the sphere exhibits minimum surface area among all the shapes. Surprisingly, in our study, we found that nanorods showed slower artemether release as compared to nanospheres. It has been reported that the nonspherical particles tend to marginate (Thompson et al., 2013) and adhere (Cooley et al., 2018) to the surfaces under the flow conditions due to their distinct shape and surface area, respectively (Chen et al., 2015). Moreover, the orientation of the particles in the dissolution medium could exert a significant impact on the available surface area for the drug release. It was attributed that the convection current might not be able to facilitate the release due to the specific orientation of the nanoparticles thus leading to the formation of a stagnant layer around the particle responsible for the slower release of the drug from the nanorods than nanospheres.

Nonspherical particles are known to alter the cellular uptake kinetics and mechanism and particle-cell interaction (Mathaes et al., 2015). Therefore, cytotoxicity of artemether loaded nanoparticles was studied to 1) understand the effect of nanosphere vs nanorods on cell viability and 2) to evaluate the biocompatibility potential of the nanorods on THP-1 monocyte cells. Cytotoxicity results showed that the transformation of nanospheres into nanorods did not produce any effect on cell viability and nanorods are suitable for the *in vivo* delivery of antimalarial drugs.

Considering that intravenous administration of artemether loaded nanorods for malaria treatment, the blood compatibility of materials was further investigated by measuring their haemolysis behaviour. Nanorods showed significantly less haemolysis of RBCs as compared to nanospheres, It could be due to the large surface of nanorods which requires less membrane bending energy as compared to the nanospheres for interaction (Zhao et al., 2011). However, the haemolysis caused by both the formulations is less than 10%.

5. Conclusion

In the present study, we reported that artemether loaded nanorods of uniform shape and narrow size distribution could be obtained using film stretching method. It was found that aspect ratio of nanorods was dictated by the film thickness, stretching extent and method of liquefaction of the particles during stretching. Drug loaded nanorods were also found to be biocompatible with THP-1 monocyte cells and RBCs. It suggested that PLGA nanorods could be used for the intravenous delivery of artemether for the treatment of cerebral malaria. Furthermore, a sustained drug release potential of nanorods could provide additional advantage of reduced dosing frequency of artemether in malaria therapy.

Author contribution

Atharva R. Bhide: Validation, Data curation, Formal analysis, Investigation, Software, Writing. **Anil B. Jindal:** Conceptualization, Funding acquisition, Resources, Investigation, Project administration, Supervision, Writing - review & editing, and finalisation of the manuscript for submission.

Declaration of Competing Interest

The authors declare that they have no known competing financial interests or personal relationships that could have appeared to influence the work reported in this paper.

Acknowledgements

Dr. Anil B. Jindal would like to acknowledge the Science and Engineering Research Board, Government of India for financial support [ECR/2018/000723].

References

Aphesteguy, J.C., Kurlyandskaya, G. V., De Celis, J.P., Safronov, A.P., Schegoleva, N.N., 2015. Magnetite nanoparticles prepared by co-precipitation method in different conditions. Mater. Chem. Phys. https://doi.org/10.1016/j.matchemphys.2015.05.044.

Arnida, Janát-Amsbury, M.M., Ray, A., Peterson, C.M., Ghandehari, H., 2011. Geometry and surface characteristics of gold nanoparticles influence their biodistribution and uptake by macrophages. Eur. J. Pharm. Biopharm. https://doi.org/10.1016/j.ejpb.2010.11.010.

Baybay, E.K., Esposito, E., Hauf, S., 2020. Pomegranate: 2D segmentation and 3D reconstruction for fission yeast and other radially symmetric cells. Sci. Rep. https://doi.org/10.1038/s41598-020-73597-w.

Belew, S., Suleman, S., Duguma, M., Teshome, H., Wynendaele, E., Duchateau, L., De Spiegeleer, B., 2020. Development of a dissolution method for lumefantrine and artemether in immediate release fixed dose artemether/lumefantrine tablets. Malar. J. https://doi.org/10.1186/s12936-020-03209-5.

Bhide, A.R., Surve, D.H., Guha, S., Jindal, A.B., 2020. A sensitive RP-HPLC method for estimation of artemether from polymeric nanoparticles after pre-column acid treatment using UV-visible detector. J. Liq. Chromatogr. Relat. Technol. https://doi.org/10.1080/10826076.2020.1777564.

Caldorera-Moore, M., Guimard, N., Shi, L., Roy, K., 2010. Designer nanoparticles: Incorporating size, shape and triggered release into nanoscale drug carriers. Expert Opin. Drug Deliv. https://doi.org/10.1517/17425240903579971.

Cao, J., Choi, J.S., Oshi, M.A., Lee, J., Hasan, N., Kim, J., Yoo, J.W., 2019. Development of PLGA micro- and nanorods with high capacity of surface ligand conjugation for enhanced targeted delivery. Asian J. Pharm. Sci. https://doi.org/10.1016/j.ajps.2018.08.008.

Castoldi, A., Empting, M., De Rossi, C., Mayr, K., Dersch, P., Hartmann, R., Müller, R., Gordon, S., Lehr, C.M., 2019. Aspherical and Spherical InvA497-Functionalized Nanocarriers for Intracellular Delivery of Anti-Infective Agents. Pharm. Res. https://doi.org/10.1007/s11095-018-2521-3.

Champion, J.A., Katare, Y.K., Mitragotri, S., 2007. Making polymeric micro- and nanoparticles of complex shapes. Proc. Natl. Acad. Sci. U. S. A. https://doi.org/10.1073/pnas.0705326104.

Champion, J.A., Mitragotri, S., 2009. Shape induced inhibition of phagocytosis of polymer particles. Pharm. Res. https://doi.org/10.1007/s11095-008-9626-z.

Chen, J., Clay, N.E., Park, N. hyung, Kong, H., 2015. Non-spherical particles for targeted drug delivery. Chem. Eng. Sci. https://doi.org/10.1016/j.ces.2014.10.022.

Cooley, M., Sarode, A., Hoore, M., Fedosov, D.A., Mitragotri, S., Sen Gupta, A., 2018. Influence of particle size and shape on their margination and wall-adhesion: implications in drug delivery vehicle design across nano-to-micro scale. Nanoscale. https://doi.org/10.1039/c8nr04042g.

Dasgupta, S., Auth, T., Gompper, G., 2014. Shape and orientation matter for the cellular uptake of nonspherical particles. Nano Lett. https://doi.org/10.1021/nl403949h.

Dendukuri, D., Tsoi, K., Hatton, T.A., Doyle, P.S., 2005. Controlled synthesis of nonspherical microparticles using microfluidics. Langmuir. https://doi.org/10.1021/la047368k.

Fish, M.B., Thompson, A.J., Fromen, C.A., Eniola-Adefeso, O., 2015. Emergence and utility of nonspherical particles in biomedicine. Ind. Eng. Chem. Res. https://doi.org/10.1021/ie504452j.

Gérard Yaméogo, J.B., Mazet, R., Wouessidjewe, D., Choisnard, L., Godin-Ribuot, D., Putaux, J.L., Semdé, R., Gèze, A., 2020. Pharmacokinetic study of intravenously administered artemisinin-loaded surface-decorated amphiphilic γ-cyclodextrin nanoparticles. Mater. Sci. Eng. C 106, 110281. https://doi.org/10.1016/j.msec.2019.110281.

Ho, C.C., Keller, A., Odell, J.A., Ottewill, R.H., 1993. Preparation of monodisperse ellipsoidal polystyrene particles. Colloid Polym. Sci. https://doi.org/10.1007/BF00657391.

Jindal, A.B., 2017. The effect of particle shape on cellular interaction and drug delivery applications of micro- and nanoparticles. Int. J. Pharm. https://doi.org/10.1016/j.ijpharm.2017.09.028.

Jindal, A.B., Devarajan, P. V., 2015. Asymmetric lipid-polymer particles (LIPOMER) by modified nanoprecipitation: Role of non-solvent composition. Int. J. Pharm. https://doi.org/10.1016/j.ijpharm.2015.04.073.

Jindal, A.B., Dighe, V.D., Surve, D.H., Jirwankar, Y.B., 2020. Long-acting efavirenz and HIV-1 fusion inhibitor peptide co-loaded polymer-lipid hybrid nanoparticles: Statistical optimization, cellular uptake, and in vivo biodistribution. Mol. Pharm. https://doi.org/10.1021/acs.molpharmaceut.0c00773.

Jurney, P., Agarwal, R., Singh, V., Choi, D., Roy, K., Sreenivasan, S.V., Shi, L., 2017. Unique size and shape-dependent uptake behaviors of non-spherical nanoparticles by endothelial cells due to a shearing flow. J. Control. Release. https://doi.org/10.1016/j.jconrel.2016.11.033.

Kolhar, P., Doshi, N., Mitragotri, S., 2011. Polymer nanoneedle-mediated intracellular drug delivery. Small. https://doi.org/10.1002/smll.201100497.

Liu, Y., Yang, G., Jin, S., Xu, L., Zhao, C.X., 2020. Development of High-Drug-Loading Nanoparticles. Chempluschem. https://doi.org/10.1002/cplu.202000496.

Makadia, H.K., Siegel, S.J., 2011. Poly Lactic-co-Glycolic Acid (PLGA) as biodegradable controlled drug delivery carrier. Polymers (Basel). https://doi.org/10.3390/polym3031377.

Makanga, M., Krudsood, S., 2009. The clinical efficacy of artemether/lumefantrine (Coartem®). Malar. J. https://doi.org/10.1186/1475-2875-8-S1-S5.

Mathaes, R., Winter, G., Besheer, A., Engert, J., 2015. Non-spherical micro- and nanoparticles: Fabrication, characterization and drug delivery applications. Expert Opin. Drug Deliv. https://doi.org/10.1517/17425247.2015.963055.

Mhatre, O., Sodha, S., 2019. Pharmaceutical feasibility and flow characteristics of polymeric non-spherical particles. Nanomedicine Nanotechnology, Biol. Med. https://doi.org/10.1016/j.nano.2019.03.002.

Pawar, J.N., Shete, R.T., Gangurde, A.B., Moravkar, K.K., Javeer, S.D., Jaiswar, D.R., Amin, P.D., 2016. Development of amorphous dispersions of artemether with hydrophilic polymers via spray drying: Physicochemical and in silico studies. Asian J. Pharm. Sci. 11, 385–395. https://doi.org/10.1016/j.ajps.2015.08.012.

Palazzo, C., Ponchel, G., Vachon, J.J., Villebrun, S., Agnely, F., Vauthier, C., 2017. Obtaining nonspherical poly(alkylcyanoacrylate) nanoparticles by the stretching method applied with a marketed water-soluble film. Int. J. Polym. Mater. Polym. Biomater. https://doi.org/10.1080/00914037.2016.1233420.

Raina, H., Kaur, S., Jindal, A.B., 2017. Development of efavirenz loaded solid lipid nanoparticles: Risk assessment, quality-by-design (QbD) based optimisation and physicochemical characterisation. J. Drug Deliv. Sci. Technol. 39, 180–191. https://doi.org/10.1016/j.jddst.2017.02.013.

Rolland, J.P., Maynor, B.W., Euliss, L.E., Exner, A.E., Denison, G.M., DeSimone, J.M., 2005. Direct fabrication and harvesting of monodisperse, shape-specific nanobiomaterials. J. Am. Chem. Soc. https://doi.org/10.1021/ja051977c.

S.K. Sahoo J. Panyam S. Prabha V. Labhasetwar Residual polyvinyl alcohol associated with poly (D 2002 J. Control. Release L-lactide-co-glycolide) nanoparticles affects their physical properties and cellular uptake 10.1016/S0168-3659(02)00127-X.

Shende, P., Desai, P., Gaud, R.S., Dhumatkar, R., 2017. Engineering of microcomplex of artemether and lumefantrine for effective drug treatment in malaria. Artif. Cells, Nanomedicine Biotechnol. https://doi.org/10.1080/21691401.2016.1267012.

Shukla, S., Seal, S., 2004. Thermodynamic tetragonal phase stability in sol-gel derived nanodomains of pure zirconia. J. Phys. Chem. B. https://doi.org/10.1021/jp037532x.

Sidhaye, A.A., Bhuran, K.C., Zambare, S., Abubaker, M., Nirmalan, N., Singh, K.K., 2016. Bio-inspired artemether-loaded human serum albumin nanoparticles for effective control of malaria-infected erythrocytes. Nanomedicine. https://doi.org/10.2217/nnm-2016-0235.

Terzopoulos, D., Fleischer, K., 1988. Modeling inelastic deformation: viscoelasticity, plasticity, fracture. Comput. Graph. doi 10 (1145/378456), 378522.

Thompson, A.J., Mastria, E.M., Eniola-Adefeso, O., 2013. The margination propensity of ellipsoidal micro/nanoparticles to the endothelium in human blood flow. Biomaterials. https://doi.org/10.1016/j.biomaterials.2013.04.011.

Truong, N.P., Whittaker, M.R., Mak, C.W., Davis, T.P., 2015. The importance of nanoparticle shape in cancer drug delivery. Expert Opin. Drug Deliv. https://doi.org/10.1517/17425247.2014.950564.

Tuteja, R., 2007. Malaria - An overview. FEBS J. https://doi.org/10.1111/j.1742-4658.2007.05997.x.

Vanka, R., Kuppusamy, G., Praveen Kumar, S., Baruah, U.K., Karri, V.V.S.R., Pandey, V., Babu, P.P., 2018. Ameliorating the in vivo antimalarial efficacy of artemether using nanostructured lipid carriers. J. Microencapsul. https://doi.org/10.1080/02652048.2018.1441915.

Wang, L., Zhou, B., Huang, S., Qu, M., Lin, Q., Gong, T., Huang, Y., Sun, X., He, Q., Zhang, Z., Zhang, L., 2019. Novel fibronectin-targeted nanodisk drug delivery system displayed superior efficacy against prostate cancer compared with nanospheres. Nano Res. https://doi.org/10.1007/s12274-019-2488-3.

Yoo, J.W., Doshi, N., Mitragotri, S., 2010. Endocytosis and intracellular distribution of PLGA particles in endothelial cells: Effect of particle geometry. Macromol. Rapid Commun. https://doi.org/10.1002/marc.200900592.

Yoo, J.W., Mitragotri, S., 2010. Polymer particles that switch shape in response to a stimulus. Proc. Natl. Acad. Sci. U. S. A. https://doi.org/10.1073/pnas.1000346107.

Yu, W., Hancock, B.C., 2008. Evaluation of dynamic image analysis for characterizing pharmaceutical excipient particles. Int. J. Pharm. https://doi.org/10.1016/j.ijpharm.2008.05.025.

Zhang, J., Wang, J., Qiao, F., Liu, Y., Zhou, Y., Li, M., Ai, M., Yang, Y., Sui, L., Zhou, Z., 2021. Polymeric non-spherical coarse microparticles fabricated by double emulsion-solvent evaporation for simvastatin delivery. Colloids Surfaces B Biointerfaces. https://doi.org/10.1016/j.colsurfb.2021.111560.

Zhao, Y., Sun, X., Zhang, G., Trewyn, B.G., Slowing, I.I., Lin, V.S.Y., 2011. Interaction of mesoporous silica nanoparticles with human red blood cell membranes: Size and surface effects. ACS Nano. https://doi.org/10.1021/nn103077k.

Zhu, X., Vo, C., Taylor, M., Smith, B.R., 2019. Non-spherical micro- and nanoparticles in nanomedicine. Mater. Horizons. https://doi.org/10.1039/c8mh01527a.

molecular pharmaceutics

pubs.acs.org/molecularpharmaceutics

Article

Evaluation of Pharmacokinetics, Biodistribution, and Antimalarial Efficacy of Artemether-Loaded Polymeric Nanorods

Atharva R. Bhide, Mansi Suri, Sapna Katnoria, Sukhbir Kaur, Yugandhara B. Jirwankar, Vikas D. Dighe, and Anil B. Jindal*

Cite This: https://doi.org/10.1021/acs.molpharmaceut.2c00507

Read Online

ACCESS | Metrics & More | Article Recommendations | Supporting Information

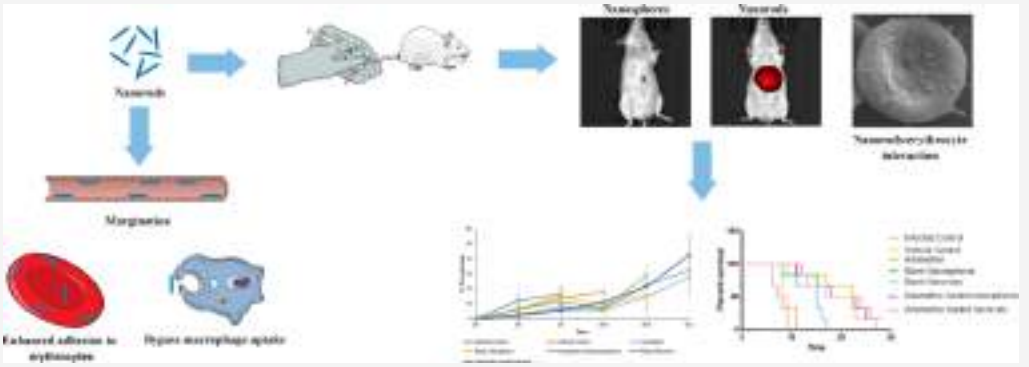

ABSTRACT: Artemether oily injection is recommended for the treatment of severe malaria by the intramuscular route. The major limitations of the artemisinin combination therapy are erratic absorption from the injection site and high dosing frequency due to a very short elimination half-life of the drug. Advanced drug delivery systems have shown significant improvement in the current malaria therapy; the desired drug concentration within infected erythrocytes is yet the major challenge. Recently, we have reported the fabrication of artemether-loaded polymeric nanorods for intravenous malaria therapy which was found to be biocompatible with THP-1 monocytes and rat erythrocytes. The objective of the present study was the evaluation of pharmacokinetics, biodistribution, and antimalarial efficacy of artemether-loaded polymeric nanorods. Scanning electron microscopy and confocal microscopy studies revealed that both nanospheres and nanorods were adsorbed onto the surface of rat erythrocytes after an incubation of 10 min. After intravenous administration to rats, artemether nanorods showed higher plasma concentration and lower elimination rate of artemether when compared with nanospheres. The biodistribution studies showed that, at 30 min, the liver concentration of DiR-loaded nanospheres was higher than that of DiR-loaded nanorods after intravenous administration to BALB/c mice. The *in vitro* schizont inhibition study showed that both nanorods and nanospheres exhibited concentration-dependent parasitic inhibition, wherein at lower concentrations (2 ppm), nanorods were more effective than nanospheres. However, at higher concentrations, nanospheres were found to be more effective. Nanorods showed higher chemosuppression on day 5 and day 7 than nanospheres and free artemether when studied with the *Plasmodium berghei* mouse model. Moreover, the survival rate of *P. berghei* infected mice was also found to be higher after treatment with artemether nanoformulations when compared with free artemether. In conclusion, polymeric nanorods could be a promising next-generation delivery system for the treatment of malaria.

KEYWORDS: *artemether, poly(lactic-co-glycolic) acid, polymeric nanoparticles, nanorods, nanoprecipitation, antimalarial, Plasmodium berghei*

INTRODUCTION

According to the WHO World Malaria Report 2021, there were an estimated 241 million malaria cases present worldwide in 2020.[1] A total of 558,000 deaths were reported due to malaria in 2019.[1] India accounted for 83% of malaria cases and 82% of all malaria deaths in the WHO South-East Asia Region. In 2020, a 68% increase in the number of deaths due to malaria was reported as compared to 2019, which was due to the disruption of the services during COVID-19.[1] The aim of the global technical strategy for malaria is at least a reduction in the malaria case incidence and mortality rate to 75% by 2025 and 90% by 2030, respectively, from the 2015 baseline. The total R&D funding for malaria was $619 million in 2020.[2]

Received: June 19, 2022
Revised: November 5, 2022
Accepted: November 7, 2022

Recently, artesunate for injection has been approved by the United States Food and Drug Administration for the initial treatment of severe malaria in adults and pediatric patients. It is administered intravenously at 0, 12, and 24 h and thereafter once daily until the patient is able to tolerate oral antimalarial therapy.[3] The major limitations of artesunate therapy are poor patient compliance due to high dosing frequency and the pain associated with parenteral administration. In the absence of artesunate, artemether is recommended for the treatment of severe malaria.[4] It is available in the market as an oily injection for intramuscular use, which showed erratic absorption of artemether from the injection site, probably due to poor solubility of the drug. Moreover, artemether exhibits a very short elimination half-life (2−3 h), which demands high dosing frequency to maintain the plasma concentration of the drug within the therapeutic range.[5] Therefore, an alternative delivery strategy is needed to overcome the limitations associated with the current antimalarial therapy.

Different advanced drug delivery systems including polymeric micro- and nanoparticles,[6−9] lipidic nanoparticles,[10−15] liposomes,[16] and micro- and nanoemulsions[17] have been exploited for the delivery of artemether with the aim to improve the present malaria therapy. The major limitations of the above formulations are rapid clearance of nanocarriers from blood circulation due to phagocytosis and the inability to maintain drug concentration within the therapeutic range inside infected erythrocytes. It has been reported that nonspherical nanoparticles could evade phagocytosis after parenteral administration[18,19] and showed significant influence on margination and wall adhesion in blood flow.[20,21] However, the role of particle shape in the improvement of antimalarial efficacy of the drugs has remained unexplored yet. Recently, we have reported the fabrication of artemether-loaded polymeric nanorods by mechanical stretching of nanospheres. Nanorods showed biocompatibility with THP-1 monocytes and rat erythrocytes. Hence, nanorods were found to be suitable for intravenous delivery of artemether.[22] Hence, the objective of the present study was the evaluation of pharmacokinetics, biodistribution, and antimalarial efficacy of artemether loaded in polymeric nanorods. The *in vivo* efficacy of artemether-loaded nanorods was studied in *Plasmodium berghei* infected mouse model.

1. MATERIALS AND METHODS

2.1. Materials. Artemether (>98.0%) was purchased from Tokyo Chemical Industry Co. Ltd. (Tokyo, Japan). Poly(lactic-*co*-glycolic) acid (75:25, MW 4000−15 000), polyvinyl alcohol (PVA, MW 9000−10 000), and coumarin-6 were purchased from Sigma-Aldrich Chemicals Company (Missouri, USA). Glutaraldehyde (25% w/w), ethylenediaminetetraacetic acid (EDTA), and curcumin (internal standard) were purchased from HiMedia Laboratories Pvt. Ltd. (Mumbai, India). Ethanol was purchased from Jabsen and Jabsen Co. (GmbH, Germany). XenoLight 1,1′-dioctadecyl-3,3,3′,3′-tetramethylindotricarbocyanine iodide [DiR, (DilC18(7))] was procured from PerkinElmer (Waltham, USA). Water was obtained from the Milli-Q system (Millipore GmbH, Germany).

2.2. Preparation and Characterization of Artemether-Loaded Poly(lactic-*co*-glycolic) Acid Nanorods. Artemether-loaded poly(lactic-*co*-glycolic) acid nanorods were prepared by mechanical stretching of nanospheres as reported previously by our group.[21] Briefly, artemether and poly(lactic-*co*-glycolic) acid were dissolved in 15 mL of acetone to prepare the organic phase. The aqueous phase was prepared by dissolving PVA (0.5% w/v) in 30 mL of warm water (65 °C). The organic phase was added slowly to the aqueous phase under continuous stirring using a magnetic stirrer, and acetone was evaporated under reduced pressure using a rotary vacuum evaporator at 37 °C. Thereafter, artemether-loaded nanosphere dispersion obtained after complete evaporation of acetone was centrifuged at 20 000 rpm for 40 min to separate polymeric nanospheres.[21] Nanospheres were freeze-dried using trehalose (10% w/v) as a cryoprotectant and stored at 4 °C until further use. To obtain artemether-loaded polymeric nanorods, 1 mL of nanosphere dispersion equivalent to 10 mg of artemether was added to 7 mL of film-forming solution (5% w/v PVA) containing glycerol (2.5% w/v) as a plasticizer. The nanosphere-embedded film [6 × 6 (cm)] was prepared from the above solution by evaporating the water at room temperature for 48 h. Thereafter, the film was incubated in preheated silicon oil (65 °C) for 15 min and was stretched at a rate of 10 mm/min in one dimension using an *in-house* film stretching apparatus. The stretched film was dissolved in water, and nanorods were harvested by centrifugation at 20 000 rpm for 40 min using an ultracentrifuge (Sorvall 150 + Micro Ultracentrifuge, Thermo Fisher Scientific, USA). The artemether-loaded nanorods were freeze-dried using trehalose (10% w/v) as a cryoprotectant and stored until further use at 4 °C. Coumarin-6- or DIR-loaded surrogate nanospheres and nanorods were prepared as described above, omitting artemether. Nanospheres were characterized for particle size and polydispersity index (PDI) using a Malvern Nano ZS (Malvern Instruments Ltd., UK), % entrapment efficiency and % drug loading were determined by estimating the drug in nanorods using the high-performance liquid chromatography-based analytical method,[23] and shape was determined by scanning electron microscopy (SEM) (FEI scanning electron microscope, Hillsboro, Washington). On the other hand, nanorods were also characterized for % drug content, major and minor Feret's diameter, major and minor axis, and aspect ratio using ImageJ software.

2.3. Interaction of Artemether-Loaded Poly(lactic-*co*-glycolic) Acid Nanorods with Rat Erythrocytes. Interaction of polymeric nanorods with erythrocytes isolated from rat blood were studied using scanning electron microscopy and confocal imaging techniques.

1.3.1. Isolation of Erythrocytes from the Rat Blood. Fresh blood (200 μL) was collected from the retro-orbital plexus, and erythrocytes were isolated from the blood by centrifugation at 1000 rpm for 5 min. Thereafter, isolated erythrocytes were washed thrice with normal saline, and 5 μL of it was redispersed in 1 mL of normal saline.

1.3.2. Scanning Electron Microscopy. Freshly prepared artemether nanospheres or artemether nanorods (10 μL) were diluted 640 times by normal saline. Thereafter, to the 500 μL of the above diluted nanodispersion, 500 μL of resuspended erythrocytes and 500 μL of 1% v/v glutaraldehyde solution were added, vortexed, and incubated for 10 min at room temperature. After incubation, an aliquot of the above solution was spread on a coverslip and dried at 37 °C. Then, the sample was chromium-coated for 45 s by placing it on a metal stub in a sputter coater (Quorum Technologies Q150TES, East Sussex, England). The images were acquired using a FEI scanning electron microscope (Hillsboro, Washington).

https://doi.org/10.1021/acs.molpharmaceut.2c00507
Mol. Pharmaceutics XXXX, XXX, XXX−XXX

1.3.3. Confocal Microscopy. Coumarin-6 (C-6)-loaded nanospheres and nanorods were used as a surrogate to study the interaction of nanoformulation with erythrocytes using confocal microscopy. Freshly prepared C-6 nanosphere or C-6 nanorod dispersion (10 μL) was diluted 640 times in normal saline, followed by incubation with the erythrocytes. After incubation with erythrocytes, the samples were fixed in 1% w/v glutaraldehyde solution, spread on a glass slide, and dried at 4 °C, followed by analysis with a laser scanning confocal microscope (ZEISS LSM 880, Axio Observer). The images were processed and analyzed with ZEN 2.3 software.

2.4. Pharmacokinetic Studies. The pharmacokinetics of artemether nanospheres and artemether nanorods were studied in Sprague-Dawley rats (250 ± 50 g) after intravenous administration. The animal study protocol was approved by the Institutional Animal Ethics Committee of Birla Institute of Technology and Science, Pilani Campus, Pilani (Protocol no.: IAEC/RES/26/04/Rev-1/29/15). The animals were fed with regular food and water *ad libitum* and were subjected to a 12 h light−dark cycle before the study. During the study, the animals were divided into two groups (n = 4). Artemether-loaded nanospheres and artemether-loaded nanorods (dose: 1.2 mg/kg) were administered to rats in group I and group II, respectively, by the intravenous route. Thereafter, 300 μL of blood was withdrawn through the retro-orbital plexus of the rat at 0, 0.08, 0.25, 0.5, 1, 2, 4, 6, 12, and 24 h in a microcentrifuge tube containing 20 μL of 10% w/v EDTA. The blood was centrifuged at 10 000 rpm for 10 min, and the plasma was separated and stored at −23 °C until further analysis. The plasma (100 μL) was spiked with 5 μL of internal standard (1 μg/mL curcumin). Artemether and curcumin were separated from the plasma by liquid−liquid extraction using dichloromethane (1 mL) as an extracting solvent. The samples were vortexed, and dichloromethane was evaporated at room temperature. Then, the samples were reconstituted using 100 μL of mobile phase. Artemether was analyzed using liquid chromatography coupled with tandem mass spectrometry (LC−MS-MS) (Waters Acquity UPLC H Class system with a Waters Xevo Triple Quadrupole mass spectrometer). Briefly, the mobile phase consisted of methanol and ammonium acetate buffer with 0.1% v/v formic acid (80: 20) with a flow rate of 0.4 mL/min and a run time of 2 min. Separation of compounds was achieved using an Acquity UPLC BEH C18 (50 mm × 2.1 mm, 1.7 μm) column. The drug and the internal standard were detected by a mass spectrometer using an ESI source. The molecular transition ions analyzed for the quantification of artemether were the artemether ammonium adduct $[M^+ + NH_4]^+$, m/z 316.02 → 267.14 and m/z 368.84 → 177 for the quantification of curcumin. The system was operated, and the data was analyzed using Mass Lynx software version 4.1.

2.5. Biodistribution Studies. DiR nanospheres and DiR nanorods were used as a surrogate to study in vivo biodistribution in BALB/c mice after intravenous administration using a PerkinElmer IVIS Lumina Series III (Waltham, USA). The procedures and protocols for the study were approved by the Institutional Animal Ethics Committee at the National Institute for Research in Reproductive Health, ICMR, Parel, Mumbai (Protocol no.: IAEC/14/19). DiR-loaded nanospheres or nanorods were administered intravenously through the tail vein of mice. Whole-body imaging of mice was carried out at different time points, including 0.5, 1, 2, 4, 8, and 24 h post-intravenous administration of nanospheres and nanorods. After 24 h, the animals were sacrificed, and the vital organs including brain, heart, kidneys, liver, lungs, female reproductive organs (F.R.O.), and spleen were isolated. The fluorescence intensity due to the presence of DIR in different organs was determined, and the % injected dose in each organ was calculated.

2.6. *In vitro* Schizont Maturation Inhibition Assay against *P. berghei* (ANKA). The *in vitro* antiplasmodial activity of artemether, artemether-loaded nanospheres, and artemether-loaded nanorods was determined by the schizont maturation inhibition assay as reported previously with modification.[24]

The stock solution of artemether was prepared in DMSO, and the formulations were prepared in PBS. These stock solutions were further diluted in incomplete medium for *in vitro* studies. Short-term *in vitro* culture of *P. berghei* ANKA blood stages was maintained using the method as reported by Trager and Jensen with modification (1976).[25]

RPMI-1640 (GIBCO) supplemented with sodium bicarbonate, antibiotics [gentamicin (50 μg/mL), penicillin (100 μg/mL), and streptomycin (100 μg/mL)], and fetal bovine serum (20%) was used for the study. The parasite was treated with artemether, artemether-loaded nanospheres, and artemether-loaded nanorods (artemether equivalent to 2, 4, and 8 μg/mL); blank nanospheres; and blank nanorods in a 24-well plate and incubated at 37 °C for 24 h. The % inhibition of schizont maturation was calculated using eq 1:

$$\%\ \text{inhibition} = \left(1 - \frac{N_{\text{drug-treated}}}{N_{\text{control}}}\right) \times 100 \quad (1)$$

where $N_{\text{drug-treated}}$ is the number of schizonts in the drug-treated well and N_{control} is the number of schizonts in the control well.

2.7. Antimalarial Efficacy of Nanoformulations in *P. berghei* Infected Mice. The procedures and protocols for the study were approved by the Institutional Animal Ethics Committee (Protocol no.: PU/45/99/CPCSEA/IAEC/2021/580) at Panjab University, Chandigarh. Female BALB/c mice (6−8 weeks) were used for the experiment. Animals were housed at room temperature (24 °C ± 1 °C) and were given food and water *ad libitum*. The erythrocyte stage of the parasite was maintained in donor (BALB/c) mice with high parasitemia (5−20%). The mice were divided into seven groups (n = 6). The animals were induced parasitemia by injecting 1.0×10^7 *Plasmodium*-infected erythrocytes *i.p.* (5−20% parasitemia). The animals were divided into groups on the basis of treatment formulation as follows: Group I (negative control), Group II (vehicle control; 0.9% normal saline), Group III (artemether free drug), Group IV (blank nanospheres), Group V (artemether-loaded nanospheres), Group VI (blank nanorods), and Group VII (artemether-loaded nanorods). The stock solutions of all the drugs were diluted in 0.9% normal saline for dosing. After 24 h of parasitemia induction, blank and artemether-loaded nanoformulations were administered intravenously at a dose of 4.8 mg/kg, while in the case of Group III, the free drug artemether (4.8 mg/kg) was administered orally as a suspension. The treatment was continued for four consecutive days. Blood (20 μL) was collected from the tail vein on predetermined time points (day 0, day 5, day 7, day 10, day 14, and day 21), and thin smears were prepared from it. The smears were air-dried, fixed with methanol, and finally stained with Giemsa stain. The average parasitemia of each

https://doi.org/10.1021/acs.molpharmaceut.2c00507
Mol. Pharmaceutics XXXX, XXX, XXX−XXX

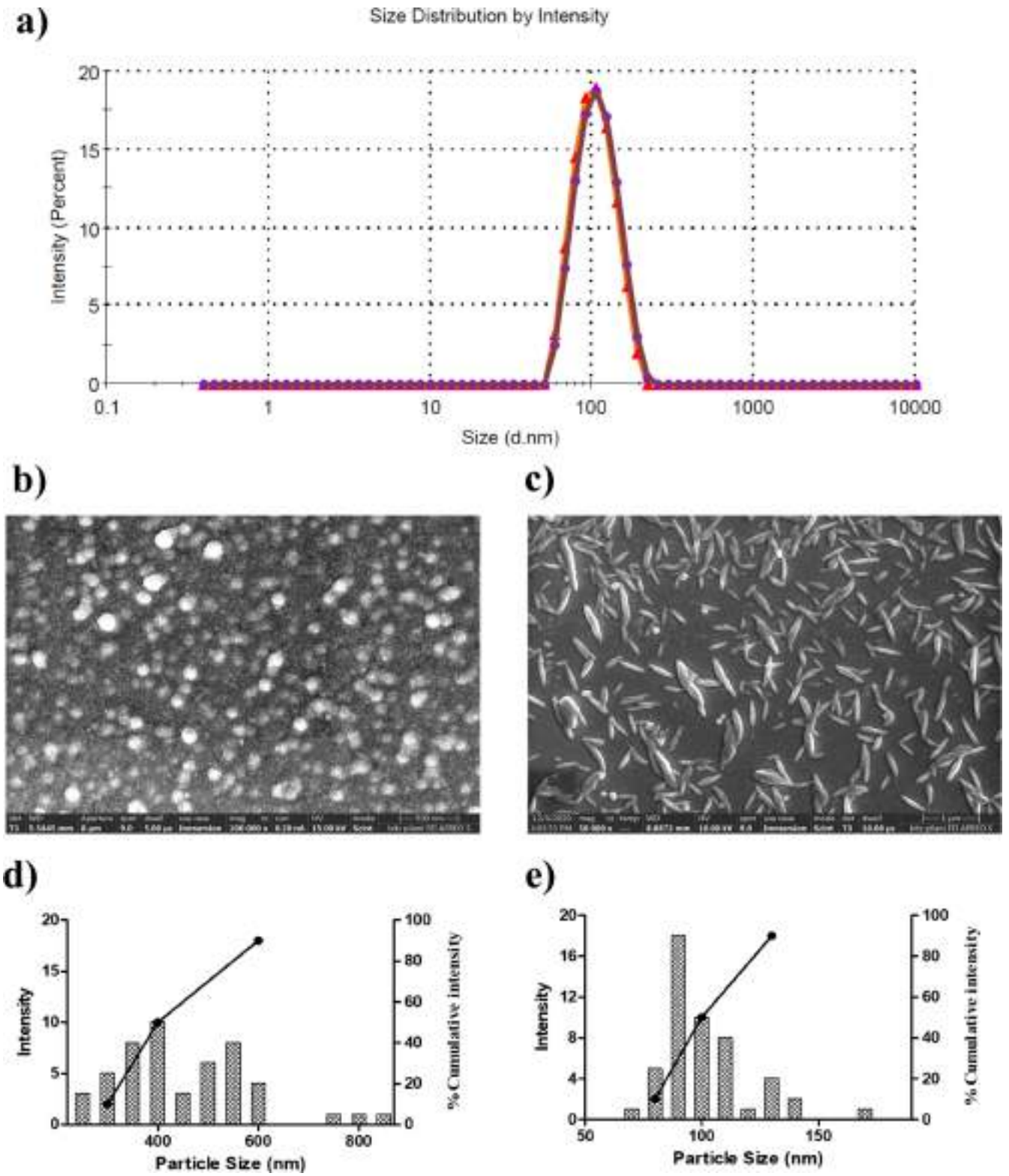

Figure 1. Characterization of nanospheres and nanorods: (a) particle size distribution of nanospheres; SEM image of (b) nanospheres and (c) nanorods; and size−frequency distribution curve of (d) major axis and (e) minor axis of nanorods.

group of mice was used to calculate the percentage reduction of parasitemia (% chemosuppression) using eq 2

$$(A - B/A) \times 100 \quad (2)$$

where A is the mean parasitemia in the negative control group and B is the parasitemia of each treated group. The mean survival time (MST) was used to assess the efficacy of the nanoformulations. Mortality was checked regularly, and the number of days from the time of inoculation of the parasite up to death were recorded for each mouse within the treatment and control groups all through a follow-up period of 28 days. Results of parasitemia and changes in survival time were

https://doi.org/10.1021/acs.molpharmaceut.2c00507
Mol. Pharmaceutics XXXX, XXX, XXX−XXX

analyzed using GraphPad Prism software version 9.3.1. for each treatment group. Two-way ANOVA and Tukey's post hoc tests were used to analyze differences between groups and subgroups, within groups, respectively. Differences were considered as statistically significant if the value is $p < 0.05$.[26]

3. RESULTS AND DISCUSSION

3.1. Preparation and Characterization of Artemether-Loaded Polymeric Nanorods. Figure 1a represents the particle size distribution of nanospheres obtained by dynamic light scattering. The SEM images of nanospheres and nanorods are presented in Figure 1b,c, respectively. The particle size distribution of the major and minor axes of nanorods is presented in Figure 1d,e, respectively. Artemether nanospheres were prepared by the standard nanoprecipitation method, and the particle size, PDI, zeta potential, % entrapment efficiency, and % drug loading of nanospheres are presented in Table 1.

Table 1. Physicochemical Properties of Nanoformulations[a]

Nanoformulation	Physicochemical properties	
Nanospheres	Particle size (nm)	101.10 ± 1.99
	PDI	0.074 ± 0.01
	Zeta potential (mV)	−24.33 ± 2.69
	% entrapment efficiency	31.83 ± 1.22
	% drug loading	3.74 ± 0.14
Nanorods	Drug content (μg/10 mg)	25.72
	Major axis (nm)	425.51 ± 133.75
	Minor axis (nm)	96.04 ± 18.55
	Major Feret's diameter (nm)	392.70 ± 103.70
	Minor Feret's diameter (nm)	100.16 ± 18.97
	Aspect ratio	4.43 ± 1.04

[a]Each value represents mean ± SD; (n = 3).

On the other hand, artemether nanorods were prepared by mechanical stretching of nanospheres using an *in-house* film stretching apparatus. During stretching, stress was experienced by the nanospheres, which was probably higher than the cohesive forces present in the polymer, leading to the elongation of spherical nanoparticles to nanorods.[21] The drug content, major axis, minor axis, major Feret's diameter, minor Feret's diameter, and aspect ratio of nanorods are also presented in Table 1. There was no significant difference observed between the major and minor axes and respective Feret's diameters of nanorods, which indicated the presence of symmetry in the particle shape (D_{90} major = 600 nm and D_{90} minor = 130 nm, D_{50} major = 400 nm and D_{50} minor = 100 nm, and D_{10} major = 300 nm and D_{10} minor = 80 nm). The D_{90}, D_{50}, and D_{10} of nanorods indicated that nanorods obtained from stretching of nanospheres were uniform in size.

3.2. Interaction of Nanoparticles with Rat Erythrocytes. Figure 2 shows the interaction of nanoparticles with rat erythrocytes. Supporting Information files SI1 and SI2 shows videos of confocal micrographs demonstrating the interaction of nanospheres and nanorods with rat erythrocytes taken from different z-positions, respectively. In the case of malaria, the parasite resides and survives within the erythrocytes. Hence, it is desirable to deliver the antimalarial drug within erythrocytes for complete eradication of the parasite. Recently, we reported that nanorods showed low hemolysis of rat erythrocytes as compared to nanospheres. However, both nanospheres and nanorods showed <10% hemolysis of rat erythrocytes.[21] In the present study, we attempted to understand the interaction of nanospheres and nanorods with erythrocytes isolated from rat blood. The interaction of nanoparticles with erythrocytes is not well understood. However, it is extremely important in the case of intravenous delivery of antimalarial formulations. SEM images revealed that both nanospheres and nanorods were adsorbed onto the surface of erythrocytes. However, due to the higher surface area of nanorods than nanospheres, the retention of nanorods on the cell surface could be more than the nanospheres in blood flow. Moreover, the particle cell interaction depends on the energy released upon interaction and the energy required for bending the cell membrane. The energy released upon interaction depends on the surface area, while the energy required for bending depends on the size of the particles. It has been reported that the higher the surface area, the higher the free energy released upon the interaction.[27] On the other hand, the lower the size, the higher the bending energy required for wrapping the particles. We, therefore, assumed that among both nanospheres and nanorods, although interacted with erythrocytes, nanorods could retain and be wrapped by the erythrocytes more efficiently than nanospheres, probably due to high surface area of nanorods.[27] It could lead to maintenance of higher concentration within the erythrocytes than the nanospheres. Nevertheless, interaction of the nanoparticles with erythrocytes needs to be studied after intravenous administration of the formulation to establish an *in vivo* proof of concept.

3.3. Pharmacokinetic Studies. The pharmacokinetic profiles of artemether-loaded nanospheres and artemether-loaded nanorods are presented in Figure 3. It was observed that in the case of artemether-loaded nanorods, the plasma drug concentration was higher when compared with that of nanospheres. Interestingly, during the initial 15 min, a rapid decrease in plasma drug concentration was observed in the case of nanospheres when compared with nanorods. The pharmacokinetic parameters of artemether nanospheres and artemether nanorods are presented in Table 2. In the case of nanospheres, the C_{max} value was found to be 1.64—fold higher than that of nanorods. A lower C_{max} in the case of artemether nanorods could result in a decrease in concentration-dependent side effects of artemether. Moreover, $t_{1/2}$ was found to be 3.09-fold higher in the case of nanorods than nanospheres. The difference in the pharmacokinetic parameters of nanorods and nanospheres after intravenous administration can be explained based on the particle shape. Higher surface area and contact angle of nanorods than nanospheres could have led to an enhanced interaction of nanoparticles with endothelial cells and erythrocytes present in the circulatory system. The enhanced interaction of the nanorods with blood components could have contributed to the higher $t_{1/2}$ of the drug in the case of nanorods. Moreover, nanorods have the ability to marginate toward the blood vessel walls, which would result in the retention of particles in the circulatory system for longer duration and creation of a depot in the blood vessel for the sustained release of drug.[28] The malaria parasite resides and survives within the erythrocyte, which emerges out from the erythrocyte into the blood after 48 h. Hence, it is desirable to maintain the plasma concentration of antimalarial drugs for an extended duration for the complete elimination of parasites from blood. Furthermore, in the case of nanorods, the AUC was also found to be 1.8-fold higher than that of nanospheres, which indicated higher exposure of the parasite to the drug after treatment with artemether nanorods when compared with the artemether nanospheres.

https://doi.org/10.1021/acs.molpharmaceut.2c00507
Mol. Pharmaceutics XXXX, XXX, XXX−XXX

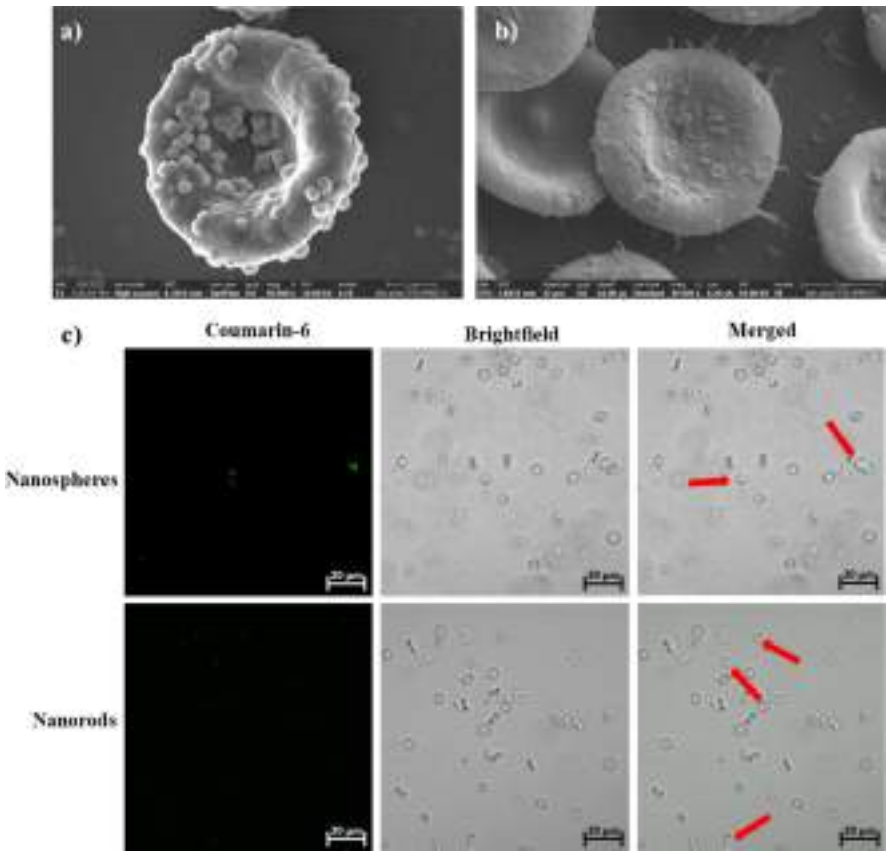

Figure 2. Erythrocyte nanoparticle interaction study. SEM image of (a) nanospheres adsorbed on erythrocytes and (b) nanorods adsorbed on erythrocytes. Confocal image of (c) nanospheres and nanorods adsorbed on erythrocytes.

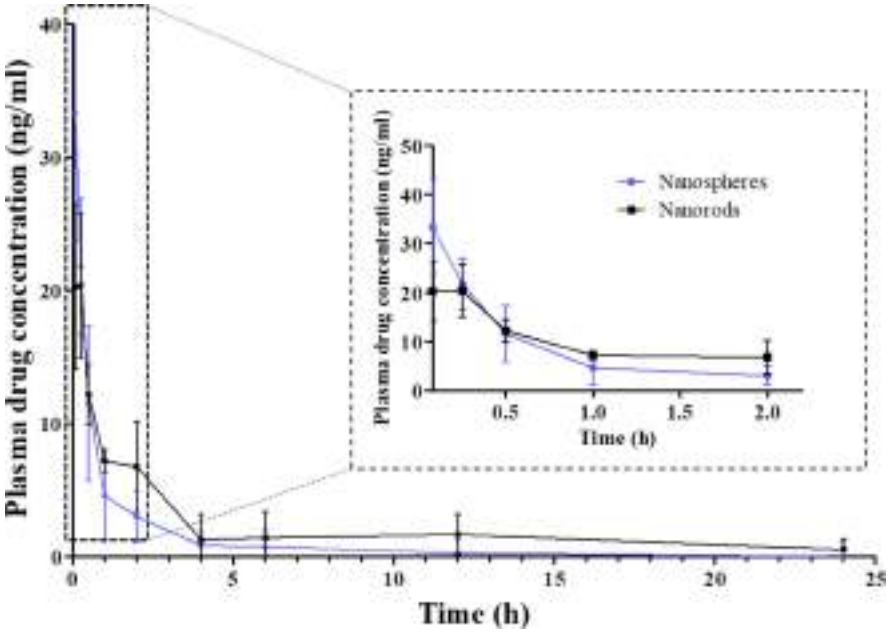

Figure 3. Pharmacokinetic profile of nanospheres (blue) and nanorods (black) after intravenous administration of artemether-loaded nanospheres and artemether-loaded nanorods.

The longer circulation time of nanorods in combination with sustained drug release could be the possible reason of higher AUC in the case of nanorods as compared to nanospheres. In the case of nanorods, their low clearance (2—fold) and high volume of distribution when compared with nanospheres indicated the presence of drug for an extended period in plasma. Comparative pharmacokinetics of nanorods and nanospheres in Sprague-Dawley rats revealed that nanorods could maintain the plasma concentration of the drug for an

https://doi.org/10.1021/acs.molpharmaceut.2c00507
Mol. Pharmaceutics XXXX, XXX, XXX−XXX

Table 2. Pharmacokinetic Parameters of Artemether-Loaded Nanospheres and Artemether-Loaded Nanorods after Intravenous Administration to Rats[a]

Pharmacokinetic parameter	Nanospheres	Nanorods
C_{max}(ng/mL)	29.33 ± 19.98	26.44 ± 10.89
$t_{1/2}$ (h)	0.43 ± 0.08	1.17 ± 0.85
AUC (ng·h/L)	12.54 ± 4.71	62.18 ± 47.03
Volume of distribution (mL/kg)	17079.45 ± 8398.52	8305.41 ± 2477.34
Clearance (mL/h/kg)	26796.44 ± 8697.65	7783.66 ± 6369.11
Mean residence time (h)	0.67 ± 0.19	5.20 ± 4.95

[a]Each value represents mean ± SD; (n = 4).

extended duration, which could lead to reduced dosing frequency.

3.4. Biodistribution Studies. A comparative biodistribution profile of DIR-loaded nanospheres and nanorods after intravenous administration is presented in Figure 4. Both nanospheres and nanorods showed a significantly higher fluorescent intensity in liver and spleen as compared to other organs. At 30 min, the liver concentration of nanorods was found to be significantly less as compared to that of nanospheres. This observation indicated that the nanorods were present in the bloodstream for a longer duration and were not phagocytosed when compared to the nanospheres. It could provide a better opportunity for nanorods to interact with erythrocytes. Moreover, an increase in the fluorescence intensity at 24 h indicates the sustained release of the dye from the nanoparticles.

3.5. *In Vitro* Schizont Maturation Inhibition Assay against *P. berghei* (ANKA). Artemether, blank nanospheres, blank nanorods, artemether-loaded nanospheres, and artemether-loaded nanorods were evaluated for inhibition of *P. berghei* schizont maturation. All the drug-loaded nanoformulations showed concentration-dependent inhibition of *P. berghei* schizont maturation. In the case of artemether, almost 70% parasite inhibition was observed at all the three concentrations. While in the case of artemether-loaded nanospheres and artemether-loaded nanorods, an increase in % parasite inhibition was observed with an increase in artemether concentration from 2 to 8 ppm. Moreover, at a lower artemether concentration, (2 ppm), nanorods showed higher % inhibition than nanospheres. While at a higher concentration (8 ppm), % inhibition of *P. berghei* schizont maturation was found to be more after incubation in nanospheres than in nanorods. Nanorods, due to their sustained drug release characteristic phenomenon, presented a slower release of artemether, which could be the possible reason for the lower % parasite inhibition of nanospheres than nanorods.[21] The % parasite inhibition with respect to different concentrations of formulations is presented in Figure 5a.

3.6. Antimalarial Efficacy of Nanoformulations in *P. berghei* Infected Mice. *3.6.1. Suppressive Activity.* The infected group (no treatment) showed the highest parasitemia, 16.75 ± 3.50% on D7, after which all the mice died. The vehicle control-treated group (Group II) showed a growth rate similar to that of the infected control group with maximum parasitemia (18.02 ± 0.76%) on day 10 after which all mice died. The *in vivo* antimalarial efficacy of artemether-loaded nanospheres and artemether-loaded nanorods showed enhanced survival and reduction in parasitemia as compared to infected control. The artemether-loaded nanospheres showed a parasite suppression of around 78.46% on the fifth day while 51.40% on the seventh day, thus indicating efficient chemosuppression when compared to the infected control. On the other hand, artemether-loaded nanorods showed an increased chemosuppression of 79.80 and 65.01% on day 5 and day 7,

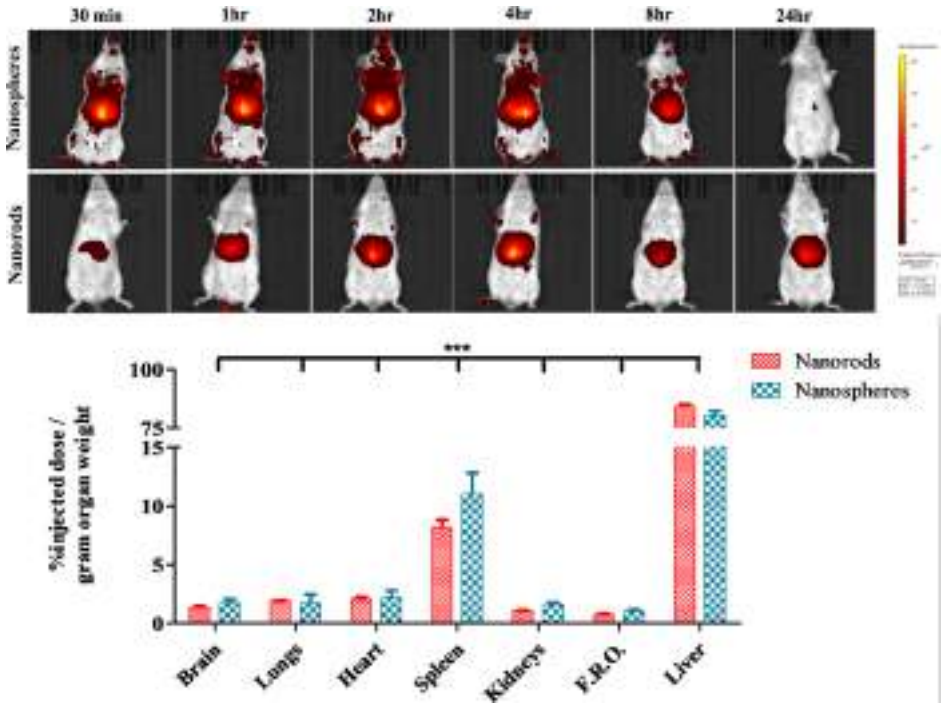

Figure 4. Biodistribution study of DiR-loaded nanoformulations. (a) Whole-body images of BALB/c mice after intravenous administration of nanospheres and nanorods and (b) comparative biodistribution profile of nanospheres and nanorods. The data was analyzed using two-way analysis of variance. The distribution of nanospheres and nanorods was significantly different among different organs (p < 0.0001).

https://doi.org/10.1021/acs.molpharmaceut.2c00507
Mol. Pharmaceutics XXXX, XXX, XXX−XXX

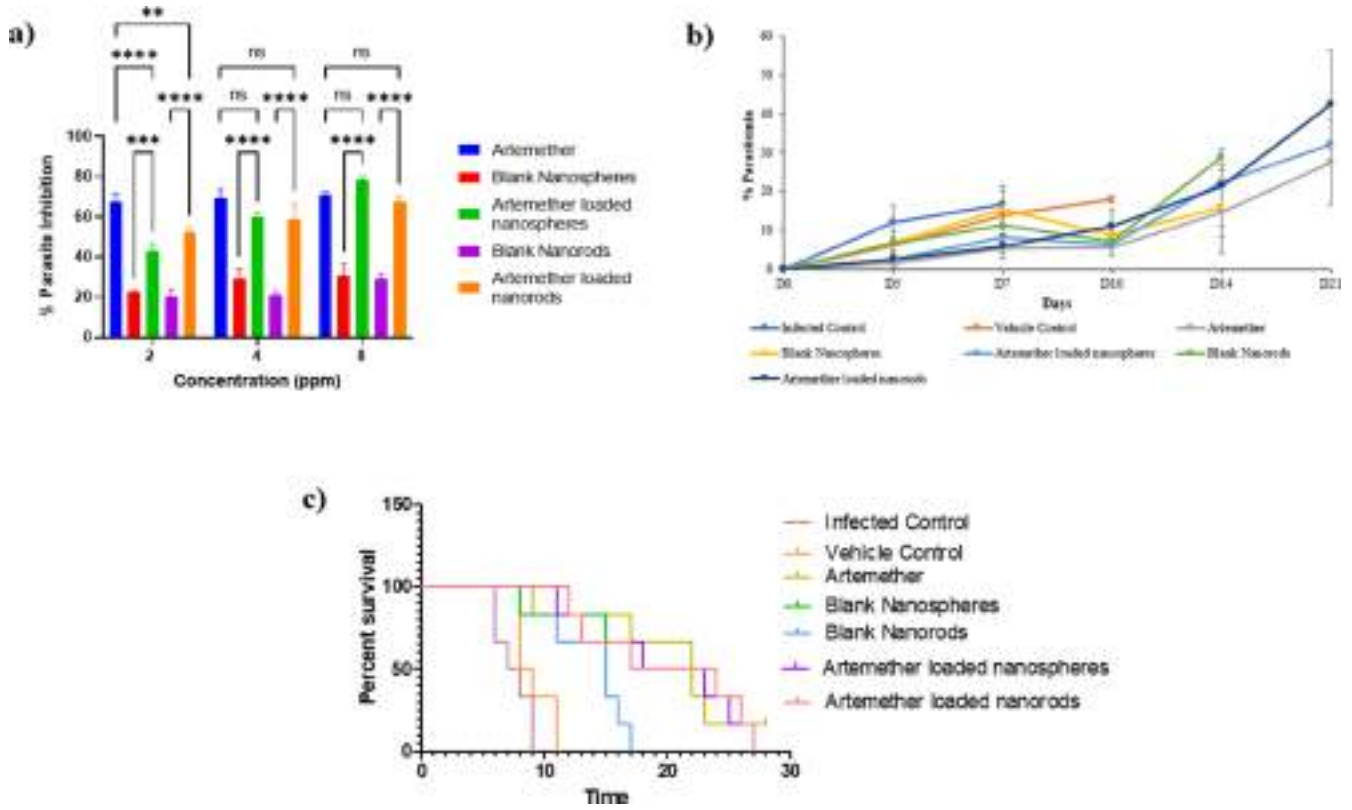

Figure 5. *In vitro* and *in vivo* antimalarial efficacy studies of artemether nanospheres and artemether nanorods: (a) *In vitro* schizont maturation inhibition by artemether, artemether nanospheres, and artemether nanorods. Results are expressed as mean ± standard deviation (S.D.) and statistically checked by two-way analysis of variance. The *p*-values in comparison to artemether with other treatment groups, blank nanospheres with artemether-loaded nanospheres, and blank nanorods with artemether-loaded rods are shown as ****$p < 0.0001$ to *$p < 0.01$ to 0.05 (significant), ns (non-significant). (b) Percent parasitemia observed in different treatment groups on different days ($n = 6$). (c) Kaplan−Meier analysis of mice in various experimental groups in suppressive test.

respectively. The higher chemosuppression in the case of nanorods could be a result of sustained drug release and longer residence time of the nanorods in the circulation. However, in both cases of nanospheres and nanorods, parasitemia was found to be increased on the 21st day, which indicated the requirement for higher doses of artemether for the complete eradication of the parasite. On the other hand, artemether (free drug) showed 5.44 ± 1.46% parasitemia on day 5 which increased to 27.49 ± 10.93% on day 21, which led to the death of animals due to high parasitemia. Only one mouse survived until day 30, which also died later due to high parasitemia. Both blank nanospheres and blank nanorods showed an increase in parasitemia as compared to artemether-loaded nanospheres and artemether-loaded nanorods (Figure 5b). The % parasitemia at determined time points and the mean survival time of the treated animals are provided in Figure 5b,c and Supporting Information 3.

3.6.2. Survival Analysis. Rise in parasitemia was evident in the infected control on day 7, after which all mice died recording an MST of 7.50 ± 1.38 days. All the mice administered with the vehicle control died by day 10, highlighting no effect of the vehicle itself in clearing the rodent malaria parasite. In the blank-treated group (nanospheres and nanorods), mortality was seen by day 21, which was statistically non-significant ($p > 0.005$) in comparison to infected control. The groups treated with artemether alone and with the formulations (nanospheres and nanorods) showed significant difference in survival rates when compared with infected control (Figure 5c).

4. CONCLUSIONS

Recently, we have reported the fabrication of artemether nanorods by mechanical stretching of artemether nanospheres. Nanorods were found to be biocompatible with rat erythrocytes and THP-1 monocytes. In the present study, both nanospheres and nanorods were adsorbed on the surface of the rat erythrocytes, indicating the enhanced potential of artemether delivery within erythrocytes. In the case of nanorods, the higher plasma concentration and lower elimination rate of artemether as compared to nanospheres suggested the possibility of reduced dosing frequency of artemether. Nanorods also showed enhanced antimalarial efficacy in the *P. berghei* mouse model, which showed the potential to improve the current malaria therapy. Hence, polymeric nanorods could be a promising next-generation delivery system for the treatment of malaria.

■ ASSOCIATED CONTENT

Supporting Information

The Supporting Information is available free of charge at https://pubs.acs.org/doi/10.1021/acs.molpharmaceut.2c00507.

Interaction of nanospheres with erythrocytes observed at different *z*-positions by confocal microscopy (MP4)

https://doi.org/10.1021/acs.molpharmaceut.2c00507
Mol. Pharmaceutics XXXX, XXX, XXX−XXX

Interaction of nanorods with erythrocytes observed at different z-positions by confocal microscopy (MP4)

Statistical significance of the in vitro and in vivo analysis of ART nanospheres and ART nanorods and development and validation of LC−MS/MS bioanalytical method for the analysis of artemether (PDF)

AUTHOR INFORMATION

Corresponding Author

Anil B. Jindal − *Department of Pharmacy, Birla Institute of Technology and Science Pilani, Jhunjhunu 333031 Rajasthan, India;* orcid.org/0000-0003-3856-869X; Phone: +911596 51 5602; Email: anil_jndl@yahoo.co.in, anil.jindal@pilani.bits-pilani.ac.in; Fax: +91 1596 244183

Authors

Atharva R. Bhide − *Department of Pharmacy, Birla Institute of Technology and Science Pilani, Jhunjhunu 333031 Rajasthan, India*

Mansi Suri − *Parasitology Laboratory, Department of Zoology, Panjab University, Chandigarh 160014 U.T., India*

Sapna Katnoria − *Parasitology Laboratory, Department of Zoology, Panjab University, Chandigarh 160014 U.T., India*

Sukhbir Kaur − *Parasitology Laboratory, Department of Zoology, Panjab University, Chandigarh 160014 U.T., India;* orcid.org/0000-0001-9071-7950

Yugandhara B. Jirwankar − *National Centre for Preclinical Reproductive and Genetic Toxicology ICMR, National Institute for Research in Reproductive Health, Mumbai 400012 Maharashtra, India*

Vikas D. Dighe − *National Centre for Preclinical Reproductive and Genetic Toxicology ICMR, National Institute for Research in Reproductive Health, Mumbai 400012 Maharashtra, India*

Complete contact information is available at: https://pubs.acs.org/10.1021/acs.molpharmaceut.2c00507

Notes

The authors declare no competing financial interest.

ACKNOWLEDGMENTS

We would like to acknowledge the Science and Engineering Research Board (SERB), Government of India, for financial support [ECR/2018/000723]. We would also like to acknowledge the Department of Science and Technology Fund for Improvement of S&T Infrastructure in Universities & Higher Educational Institutions (DST-FIST) for the LC−MS/MS facility.

ABBREVIATIONS

AR, aspect ratio; EDTA, ethylenediaminetetraacetic acid; FBS, fetal bovine serum; HPLC, high-performance liquid chromatography; UPLC, ultra-performance liquid chromatography; MST, mean survival time; PMA, phorbol 12-myristate 13-acetate; PVA, polyvinyl alcohol; SD, standard deviation; C_{max}, maximum plasma drug concentration; AUC, area under the curve; $t_{1/2}$, half-life; V_d, volume of distribution

REFERENCES

(1) World Health Organization. *World Malaria Report 2020*, 2020. Malaria report.

(2) https://www.statista.som/statistics/266958/research-and-development-funding-for-diseases-worldwide/ (Accessed on 14/06/2022).

(3) https://www.accessdata.fda.gov/drugsatfda_docs/label/2022/213036orig1s001lbl.pdf (Assessed on 14/06/2022).

(4) *Guidelines for the Treatment of Malaria*, 3rd ed.; World Health Organization, 2022 (Assessed on 14/06/2022).

(5) Bhandari, S.; Bhandari, V.; Sood, J.; Jaswal, S.; Rana, V.; Bedi, N.; Sehgal, R.; Tiwary, A. K. Improved pharmacokinetic and pharmacodynamic attributes of artemether-lumefantrine-loaded solid SMEDDS for oral administration. *J. Pharm. Pharmacol.* **2017**, *69*, 1437−1446.

(6) Sidhaye, A. A.; Bhuran, K. C.; Zambare, S.; Abubaker, M.; Nirmalan, N.; Singh, K. K. Bio-Inspired Artemether-Loaded Human Serum Albumin Nanoparticles for Effective Control of Malaria-Infected Erythrocytes. *Nanomedicine* **2016**, *11*, 2809−2828.

(7) Gérard Yaméogo, J. B.; Mazet, R.; Wouessidjewe, D.; Choisnard, L.; Godin-Ribuot, D.; Putaux, J. L.; Semdé, R.; Gèze, A. Pharmacokinetic study of intravenously administered artemisinin-loaded surface-decorated amphiphilic γ-cyclodextrin nanoparticles. *Mater. Sci. Eng. C* **2020**, *106*, 110281.

(8) Mangrio, F. A.; Dwivedi, P.; Han, S.; Zhao, G.; Gao, D.; Si, T.; Xu, R. X.Characteristics of Artemether-Loaded Poly(Lactic-Co-Glycolic) Acid Microparticles Fabricated by Coaxial Electrospray: Validation of Enhanced Encapsulation Efficiency and Bioavailability. *Mol. Pharm.***2017**, *14*, DOI: 10.1021/acs.molpharmaceut.7b00862.

(9) Yaméogo, J. B. G.; Gèze, A.; Choisnard, L.; Putaux, J. L.; Gansané, A.; Sirima, S. B.; Semdé, R.; Wouessidjewe, D.Self-Assembled Biotransesterified Cyclodextrins as Artemisinin Nanocarriers - I: Formulation, Lyoavailability and in Vitro Antimalarial Activity Assessment. *Eur. J. Pharm. Biopharm.***2012**, *80*. DOI: 10.1016/j.ejpb.2011.12.007

(10) Nnamani, P. O.; Hansen, S.; Windbergs, M.; Lehr, C. M.Development of Artemether-Loaded Nanostructured Lipid Carrier (NLC) Formulation for Topical Application. *Int. J. Pharm.***2014**, *477*. DOI: 10.1016/j.ijpharm.2014.10.004

(11) Prabhu, P.; Suryavanshi, S.; Pathak, S.; Sharma, S.; Patravale, V. Artemether-lumefantrine nanostructured lipid carriers for oral malaria therapy: Enhanced efficacy at reduced dose and dosing frequency. *Int. J. Pharm.* **2016**, *511*, 473−487.

(12) Prabhu, P.; Suryavanshi, S.; Pathak, S.; Patra, A.; Sharma, S.; Patravale, V.Nanostructured lipid carriers of artemether-lumefantrine combination for intravenous therapy of cerebral malaria. *Int. J. Pharm.***2016**, *513*. DOI: 10.1016/j.ijpharm.2016.09.008

(13) Patil, J.; Rajput, R.; Nemade, R.; Naik, J. Preparation and Characterization of Artemether Loaded Solid Lipid Nanoparticles: A 32 Factorial Design Approach. *Mater. Technol.* **2020**, *35*, 719−726.

(14) Parashar, D.; Aditya, N. P.; Murthy, R. S. R. Development of Artemether and Lumefantrine Co-Loaded Nanostructured Lipid Carriers: Physicochemical Characterization and in Vivo Antimalarial Activity. *Drug Deliv.* **2016**, *23*, 123−129.

(15) Jain, K.; Sood, S.; Gowthamarajan, K. Optimization of Artemether-Loaded NLC for Intranasal Delivery Using Central Composite Design. *Drug Deliv.* **2015**, *22*, 940−954.

(16) Isacchi, B.; Arrigucci, S.; la Marca, G.; Bergonzi, M. C.; Vannucchi, M. G.; Novelli, A.; Bilia, A. R.Conventional and Long-Circulating Liposomes of Artemisinin: Preparation, Characterization, and Pharmacokinetic Profile in Mice. *J. Liposome Res.***2011**, *21*. DOI: 10.3109/08982104.2010.539185

(17) Ma, Y.; Lu, T.; Zhao, W.; Wang, Y.; Chen, T.; Mei, Q.; Chen, T.Enhanced Antimalarial Activity by a Novel Artemether-Lumefantrine Lipid Emulsion for Parenteral Administration. *Antimicrob. Agents Chemother.***2014**, *58*. DOI: 10.1128/AAC.01428-13

(18) Jindal, A. B.The Effect of Particle Shape on Cellular Interaction and Drug Delivery Applications of Micro- and Nanoparticles. *Int. J. Pharm.***2017**, *532*. DOI: 10.1016/j.ijpharm.2017.09.028

(19) Devarajan, P. V.; Jindal, A. B.; Patil, R. R.; Mulla, F.; Gaikwad, R. V.; Samad, A. Particle Shape: A New Design Parameter for Passive

Targeting In Splenotropic Drug Delivery. *J. Pharm. Sci.* **2010**, *99*, 2576−2581.
(20) Jurney, P.; Agarwal, R.; Singh, V.; Choi, D.; Roy, K.; Sreenivasan, S. V.; Shi, L.Unique Size and Shape-Dependent Uptake Behaviors of Non-Spherical Nanoparticles by Endothelial Cells Due to a Shearing Flow. *J. Controlled Release***2017**, *245*. DOI: 10.1016/j.jconrel.2016.11.033
(21) Guha, S.; Jindal, A. B.An Insight into Obtaining of Non-Spherical Particles by Mechanical Stretching of Micro- and Nano-spheres. *J. Drug Deliv. Sci. Technol.***2020**, *59*. DOI: 10.1016/j.jddst.2020.101860
(22) Bhide, A. R.; Jindal, A. B. Fabrication and Evaluation of Artemether Loaded Polymeric Nanorods Obtained by Mechanical Stretching of Nanospheres. *Int. J. Pharm.* **2021**, *605*, 120820.
(23) Bhide, A. R.; Surve, D. H.; Guha, S.; Jindal, A. B.A Sensitive RP-HPLC Method for Estimation of Artemether from Polymeric Nanoparticles after Pre-Column Acid Treatment Using UV-Visible Detector. *J. Liq. Chromatogr. Relat. Technol.***2020**, *43*. DOI: 10.1080/10826076.2020.1777564
(24) World Health Organization (WHO). *CTD/MAL/ 97, 20*: Geneva, 2001.
(25) Trager, W.; Jensen, J. B. Human Malaria Parasites in Continuous Culture. *Science* **1976**, *193*, 673−675.
(26) Knight, D. J.; Peters, W. The antimalarial activity of N-benzyloxydihydrotriazines. *Ann. Trop. Med. Parasitol.* **1980**, *74*, 393−404.
(27) Brenner, J. S.; Pan, D. C.; Myerson, J. W.; Marcos-Contreras, O. A.; Villa, C. H.; Patel, P.; Hekierski, H.; Chatterjee, S.; Tao, J. Q.; Parhiz, H.; Bhamidipati, K.; Uhler, T. G.; Hood, E. D.; Kiseleva, R. Y.; Shuvaev, V. S.; Shuvaeva, T.; Khoshnejad, M.; Johnston, I.; Gregory, J. V.; Lahann, J.; Wang, T.; Cantu, E.; Armstead, W. M.; Mitragotri, S.; Muzykantov, V.Red Blood Cell-Hitchhiking Boosts Delivery of Nanocarriers to Chosen Organs by Orders of Magnitude. *Nat. Commun.***2018**, *9*(). DOI: 10.1038/s41467-018-05079-7
(28) Da Silva-Candal, A.; Brown, T.; Krishnan, V.; Lopez-Loureiro, I.; Ávila-Gómez, P.; Pusuluri, A.; Pérez-Díaz, A.; Correa-Paz, C.; Hervella, P.; Castillo, J.; Mitragotri, S.; Campos, F. Shape Effect in Active Targeting of Nanoparticles to Inflamed Cerebral Endothelium under Static and Flow Conditions. *J. Controlled Release* **2019**, *309*, 94−105.

https://doi.org/10.1021/acs.molpharmaceut.2c00507
Mol. Pharmaceutics XXXX, XXX, XXX−XXX